

PREDICTING CENSUS SURVEY RESPONSE RATES WITH PARSIMONIOUS ADDITIVE MODELS AND STRUCTURED INTERACTIONS

BY SHIBAL IBRAHIM^{1,*}, PETER RADCHENKO^{2,‡}, EMANUEL BEN-DAVID^{3,§}, AND RAHUL MAZUMDER^{1,†}

¹Massachusetts Institute of Technology, *shibal@mit.edu; †rahulmaz@mit.edu

²University of Sydney, ‡peter.radchenko@sydney.edu.au

³United States Census Bureau, §emanuel.ben.david@census.gov

In this paper we consider the problem of predicting survey response rates using a family of flexible and interpretable nonparametric models. The study is motivated by the US Census Bureau’s well-known ROAM application which uses a linear regression model trained on the US Census Planning Database data to identify hard-to-survey areas. A crowdsourcing competition (Erdman and Bates, 2016) organized around ten years ago revealed that machine learning methods based on ensembles of regression trees led to the best performance in predicting survey response rates; however, the corresponding models could not be adopted for the intended application due to their black-box nature. We consider nonparametric additive models with small number of main and pairwise interaction effects using ℓ_0 -based penalization. From a methodological viewpoint, we study both computational and statistical aspects of our estimator; and discuss variants that incorporate strong hierarchical interactions. Our algorithms (opensourced on github) extend the computational frontiers of existing algorithms for sparse additive models, to be able to handle datasets relevant for the application we consider. We discuss and interpret findings from our model on the US Census Planning Database. In addition to being useful from an interpretability standpoint, our models lead to predictions that appear to be better than popular black-box machine learning methods based on gradient boosting and feedforward neural networks – suggesting that it is possible to have models that have the best of both worlds: good model accuracy and interpretability.

1. Introduction. Sample surveys and censuses are primary data sources in social science studies. However, low and often unpredictable response rates in surveys remain a continual source of concern (Erdman and Bates, 2016; Smith, 2014; Tourangeau et al., 2014) – see Figure 1 for an illustration on the American Community Survey. Tourangeau et al. (2014) discuss a multitude of factors that make parts of the population hard-to-survey – such factors are often used to improve sampling strategies, questionnaire designs, recruitment methods, and the language in which the interview is conducted, among others. Erdman and Bates (2016) emphasize the usefulness of having an indicator for hard-to-survey areas to guide targeted surveying (including oversampling), staff recruitment strategies, and targeted follow-ups for non-responders. For major campaigns such as the decennial US Census, this approach can help guide resource allocation for advertisements and building community partnership activities. Eliciting responses from non-self-responding households through follow-up operations can be very costly and time consuming. The Census Bureau estimates that a single percentage increase in the self-response rate amounts to roughly 85 million dollars saved in personal

Keywords and phrases: Population surveys, low-response score, Nonparametric additive models with interactions, sparsity, hierarchical sparsity, large scale optimization, integer programming.

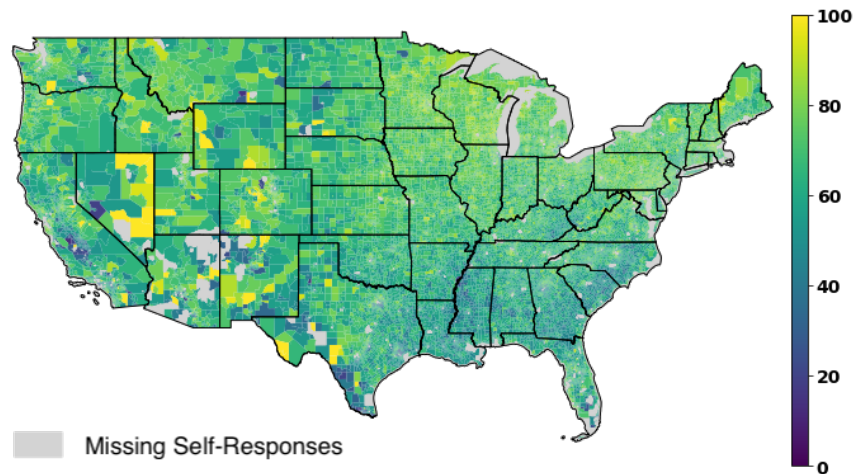


Fig 1: The 2013-2017 American Community Survey self-response rates for all tracts in the continental United States. The North in general, and the Upper Midwest and the Northeast in particular, have higher self-response rates than the rest of the country. Tracts with lower self-response rates are visible in many states – in particular, in the South and in the Mountain region.

follow-up costs (US Census Bureau, 2009; Bates and Mulry, 2011). Apart from the cost, the quality of proxy enumerations and imputations is typically significantly lower than that of self-responses (Mule, 2012).

Both the UK Office for National Statistics and the US Census Bureau have created measures that help quantify the difficulty in gathering data across different geographic areas. A report by Bruce, Robinson and Sanders (2001) from the US Census Bureau introduced a hard-to-count (HTC) score for identifying difficult to enumerate segments of the population. The HTC score, which is based on 12 carefully chosen covariates (for example, housing variables and socio-demographic/economic indicators) has found its use in the planning for the 2010 Census and many other national surveys. The HTC score, however, has some limitations and was later improved to the low-response-score, or LRS (Erdman and Bates, 2016). The LRS plays a key role in the US Census Bureau’s Response Outreach Area Mapper (ROAM) application¹ to identify hard-to-survey areas. The LRS appears to have been partly motivated by the 2012 nationwide competition, organized by the Census Bureau in partnership with Kaggle, on predicting the mail-return rates. This competition aimed to solicit models highly predictive of the decennial census response rates, easily replicable, inherently interpretable, and consistent for use in the field at various levels of geography. Even though the winning models from the competition had good predictive performance, they lacked *reproducibility* and *interpretability*. Some of the winning models included covariates that are not publicly available; in particular, they were not chosen from within the US Census Bureau Planning Database. Additionally, the winning models included covariates that were good predictors but not actionable². Interpretability suffered due to a multitude of factors. First, the winning models were based on complex ensemble methods (for example, random forests and gradient boosting). Second, these methods employed a large number of covariates (the best model had nearly 340), which hurt the model parsimony. After careful analysis, Erdman and Bates (2016) proposed a linear model based on 25 covariates – LRS is the prediction

¹<https://www.census.gov/library/visualizations/2017/geo/roam.html>

²These include covariates such as the nearest neighboring block group return rates and margins of error for various estimates. Models that incorporate such features are not actionable.

from this model. While this model suffered in terms of predictive accuracy compared to the black-box machine learning methods, it was highly interpretable and led to useful actionable insights. For example, Erdman and Bates highlight three different block-groups (Columbia Heights, Trinidad, Anacostia) in the District of Columbia that have similar LRS predictions but their characteristics vary, indicating a need for different actions to increase self-response. Columbia Heights has a large Hispanic population, suggesting they could benefit from forms and advertising in Spanish. Anacostia has a stable population (low relocation to the region) and could benefit from community partnerships. On the other hand, Trinidad is characterized as a region in transition with high mobility of the young population. This area could potentially benefit from web-based advertisements for internet-based responses from the tech-savvy younger population.

We aim to predict self-response rates across all Census tracts in the US using operational, socio-economic, and demographic characteristics from the US Census Planning Database. Our goal is to propose interpretable statistical models that deliver strong predictive performance and, thus, can be used to complement the currently used LRS metric. Our hope is that these models lend operational insights into factors influencing survey self-response rates to facilitate the downstream goal of having a cost-effective census with improved coverage.

Statistical models. We propose estimators based on Additive Models (Hastie and Tibshirani, 1987; Hastie, Tibshirani and Friedman, 2001), or AMs, with smooth nonlinear components that include nonlinear pairwise interactions between covariates. Given response $y \in \mathbb{R}$ and feature-vector $\mathbf{x} := (x_1, \dots, x_p) \in \mathbb{R}^p$, we model the conditional mean function as

$$(1) \quad \mathbb{E}(y|\mathbf{x}) = \sum_{j \in [p]} f_j(x_j) + \sum_{j < k} f_{j,k}(x_j, x_k),$$

where f_j and $f_{j,k}$ are unknown smooth univariate and bivariate functions, respectively. Drawing inspiration from linear model settings (Bach et al., 2012), we propose new methodology to estimate the unknown functional components via an optimization problem with structural constraints arising from interpretability considerations. To obtain a sparse model with few predictors, that is, with many of the components $\{f_j\}$ and $\{f_{j,k}\}$ estimated as exactly zero, we present a novel ℓ_0 -regularized approach³, penalizing the number of nonzero components in the model. In addition, we explore a refined notion of interpretability in the context of interaction modeling – namely, hierarchical sparsity – inspired by its usage in linear models (for example, Bien, Taylor and Tibshirani, 2013; Hazimeh and Mazumder, 2020b). To our knowledge, we present a novel exploration of computational and statistical perspectives of an ℓ_0 regularized approach for fitting sparse additive models with pairwise interactions.

Applied contributions. Our empirical analysis on the US Census Bureau Planning Database demonstrates the promise of our proposed approach as a potential tool to predict self-response rates in the US Census Bureau application.

Our approach leads to improved prediction of the self-response rates when compared to the linear regression methods discussed in the US Census Bureau report. The improvements are due to *both* the departure from linearity and the presence of nonlinear interactions. Importantly, the prediction accuracy of our flexible models appears to be at par with (or slightly better than) black-box machine learning methods such as neural networks and gradient boosted decision trees, which topped the nationwide Kaggle competition organized by the Census Bureau.

³For examples of ℓ_0 -based approaches and illustrations of their advantages over the ℓ_1 -based counterparts in the context of linear regression, see Bertsimas, King and Mazumder (2016); Mazumder and Radchenko (2017); Mazumder, Radchenko and Dedieu (2017); Hazimeh and Mazumder (2020a) and the references therein.

Our framework results in simple models and allows for automated variable selection. Our models are substantially more compact than many competing benchmarks – we use 8-20 times fewer interaction effects than the corresponding linear models, and about half as many covariates as off-the-shelf machine learning methods (e.g, gradient boosting, feedforward neural networks, or explainable boosting machines) or the sparse *linear* models with interaction effects. Our models also use a fewer number of covariates (by about 30%) compared to sparse nonparametric additive models (without interactions). We use our models to gather useful operational insights into the factors that influence response rates in surveys across different segments of the population. In particular, our models automatically identify interactions between many of the key factors that have been used in prior publications from the Census Bureau (Bates and Mulry, 2011) to derive meaningful clustering of the population. These interaction effects appear to result in improved predictions of survey response rates and help complement the existing studies by the Census Bureau (Bates and Mulry, 2011; Kulzick et al., 2019) on understanding different segments of the population. In summary, our work appears to address many of the challenges of the US Census application by delivering parsimonious models with good predictive performance.

Methodological contributions. We propose a new family of estimators based on nonparametric additive models with interactions under combinatorial constraints that promote parsimony and interpretability. We establish statistical guarantees for the resulting estimators and present large-scale algorithms to compute these estimators – these algorithms significantly expand the current computational landscape for nonparametric additive models with pairwise interactions. Our approach addresses some of the key computational challenges posed by the large-scale setting of the Census dataset, with $\approx 10^5$ nonparametric interaction components and $\approx 10^5$ observations. The code implementing our algorithms is available at <https://github.com/ShibalIbrahim/Additive-Models-with-Structured-Interactions>.

Related Work. There is an impressive body of methodological and theoretical work on using convex ℓ_1 -based approaches to fit sparse nonparametric AMs without interactions (see, for example, Meier, van de Geer and Bühlmann, 2009; Ravikumar et al., 2009; Huang, Horowitz and Wei, 2010; Zhao and Liu, 2012; Yuan and Zhou, 2016, and the references therein). Even with main-effects alone, these convex optimization-based methods face computational challenges for the problem-scales we seek to address⁴. This possibly limits practitioners from realizing the full potential of nonparametric AMs in large-scale settings arising in various practical applications. In terms of statistical properties, the ℓ_0 -based estimators can offer improvements over their ℓ_1 -counterparts, both on the prediction and the model selection fronts. To this end, we refer the reader to recent work by Hazimeh, Mazumder and Radchenko (2023) demonstrating the advantages of using the ℓ_0 -regularized framework for grouped variable selection (which includes nonparametric AMs) *without* interactions.

In the presence of pairwise interactions, a setting we focus on, the problem of variable selection in nonparametric AMs becomes considerably more challenging. The approaches by Meier, van de Geer and Bühlmann (2009) and Ravikumar et al. (2009) consider additive models with main effects but no pairwise interactions. Lin and Zhang (2006) introduced COSSO, which is a well-known method to fit model (1); however, the method appears to be suitable for low-dimensional settings – for example, the authors consider instances with $n \sim 500$, $p \sim 10$, and ~ 50 pairwise interactions⁵.

⁴Based on our experience, currently available software (for example, R package SAM) encounters numerical difficulties for instances where n is on the order of thousands, and p is on the order of hundreds.

⁵There appears to be no open-source implementation for COSSO.

COSMO penalizes the sum of the Sobolev norms of the functional components in representation (1) and, thus, is capable of producing sparse models. However, the convex COSMO penalty jointly controls sparsity and smoothness, potentially resulting in unwanted shrinkage interfering with component selection. In contrast, our proposed approach uses separate penalties for smoothness and sparsity, and encourages sparsity *directly* via an ℓ_0 -based penalty on the number of components in the model.

More recently, some methods have been proposed that extend the scope of classical non-parametric AMs (Hastie and Tibshirani, 1987). In a series of works Lou et al. (2013); Nori et al. (2019); Yang, Zhang and Sudjianto (2021) explore tree-based and neural-network-based approaches for fitting additive models with sparse interactions. Lou et al. (2013) propose a two-stage approach using shallow tree-like models for the main and interaction effects. In the first stage, they use gradient boosting to fit the main effects – the boosting procedure cycles through all features in a round-robin fashion to fit *all* main effects. In the second stage, they use a scheme to select a small subset of pairwise interactions—these interaction effects are fitted with shallow tree-like models via gradient boosting. Nori et al. (2019) provide an efficient implementation of the above approach as Explainable Boosting Machines (EBM) in the well-known *interpretml* toolkit. The EBM procedure is not based on optimizing a penalized estimation framework and, to our knowledge, no statistical guarantees for it are known.

In another line of work, Yang, Zhang and Sudjianto (2021) proposed GAMI-Net, which uses neural networks to fit main and pairwise interaction effects. GAMI-Net uses multi-stage approach: (i) fit all main effects, where each main effect is modeled using a multi-layer perceptron (MLP); (ii) select Top- k interactions based on an interaction detection method (Lou et al., 2013) on the residuals; (iii) fit the Top- k interaction effects simultaneously, where each interaction effect is again modeled as MLP; (iv) fine-tune all selected main effects and interaction effects jointly. GAMI-Net also prunes some components in steps (i) and (iii) based on some ranking measure. Like EBM, the GAMI-Net method does not solve a penalized optimization criterion; no theoretical statistical guarantees for this method are known.

Zschech et al. (2022) independently compared various existing interpretable models and concluded that EBM (Nori et al., 2019) and GAMI-Net (Yang, Zhang and Sudjianto, 2021) appear to be the leading interpretable models. However, both models have some practical limitations. For example, EBM includes all main effects in the model (i.e., there is no feature selection). Neural-based approaches, such as GAMI-Net, are quite computationally expensive. On the Census dataset that we consider, GAMI-Net takes 3 days (using a 8-CPU machine) to compute one model if we consider 1000 tuning parameters, we are looking at a steep 3000 days of computation cost.

To the best of our knowledge, our algorithmic framework for sparse nonparametric AMs with interactions is novel and is likely to be of independent interest from a computational methodology perspective in applications beyond the one studied herein.

Organization. Section 2 presents the statistical models pursued in this paper. Section 2.3 investigates the statistical properties of our proposed estimators. Section 2.4 discusses how to obtain solutions to the corresponding large-scale discrete optimization problems. Section 3 develops an extension of our method that incorporates strong hierarchy constraints. In Section 4, we present simulation studies comparing our methods with COSMO, EBM and GAMI-Net. Section 5 discusses numerical results for the US Census Bureau application that motivates this study. Additional technical details are provided in the supplementary material.

2. Statistical Models and Methodology. We now discuss the statistical models we pursue in this work. Section 2.1 gives an overview of AMs with nonlinear main effects and pairwise interactions, along with optimization formulations associated with the estimation procedures. Section 2.2 presents our new models to incorporate sparsity in the main and interaction effects.

2.1. *Smooth additive models with pairwise interactions.* Given data $\{(y_i, \mathbf{x}_i)\}_1^n$, our key objective is to learn a multivariate conditional mean function $f(\mathbf{x}) := \mathbb{E}(y|\mathbf{x})$, where $f: \mathbb{R}^p \mapsto \mathbb{R}$ is an unknown smooth function (Wahba, 1990). It is well known that such functions become difficult to estimate even for moderately high p due to the curse of dimensionality – therefore we will focus on a smaller class of models corresponding to additive structures (Hastie and Tibshirani, 1987; Stone, 1986). A popular approach considered in the literature estimates a nonparametric additive model containing main-effects only, with $f(\mathbf{x}) = \sum_{j=1}^p f_j(x_j)$, where each f_j is an unknown univariate smooth function of the j -th coordinate in \mathbf{x} , namely x_j . In various applications, however, nonparametric AMs based on main effects alone may not lead to a sufficiently rich representation for predicting the outcome of interest: including interaction terms can lead to better predictive models while remaining interpretable to a practitioner (Hastie and Tibshirani, 1987). AMs with pairwise interactions are a useful tool in applied statistical modeling with various applications in medical sciences and healthcare, e-commerce applications, recommender system problems, and sentiment analysis, among others (Hastie, Tibshirani and Wainwright, 2015).

The need for interactions. Exploratory analysis on US Census Planning Database Tract dataset suggests that interaction effects across features can lead to improved predictions of the survey self-response rate. For example, there is interaction between the percentages of “People who do not speak English well” and “Renters” in the area. In areas with a relatively high concentration of poor English speakers (e.g., $\geq 5.4\%$), the self-response rate decreases on an average by 0.33% for a unit increase in the percentage of renters. On the other hand, when the concentration of poor English speakers is relatively low (e.g., $\leq 1.6\%$), the self-response rate decreases at the rate of 0.21%. Similarly, there is a strong interaction effect between covariates “Single-unit households” and “Household moved in 2010 or later” in terms of predicting the low self-response rate. Indeed, Erdman and Bates (2016) note the importance of incorporating interaction effects when predicting the self-response rate, although the paper does not pursue statistical modeling involving interactions.

An additive model with nonlinear main effects and pairwise interactions extends the traditional AM framework with main effects alone (Hastie, Tibshirani and Friedman, 2001; Radchenko and James, 2010), and is given by model (1), where the unknown components $\{f_j\}$ and $\{f_{j,k}\}$ need to be estimated from the data. This leads to two key challenges. The presence of $O(p^2)$ -many unknown nonparametric functions results in statistical challenges even for a moderate value of p . Additional regularization (for example, in the form of sparsity in the components) may be necessary to obtain a reliable statistical model with good generalization properties (cf Section 2.2). Furthermore, as we mention in Section 1, estimating model (1) leads to severe computational challenges for large problems (for example, those with $n \approx 10^5$ and $p^2 \approx 10^5$, similar to the instances we consider in our applications) – we discuss how we address these challenges in Section 2.4.

We assume that the components $\{f_j\}$ and $\{f_{j,k}\}$ are smooth (for example, twice continuously differentiable). For illustration, consider Figure 2, which shows that the marginal fits for the self-response rate appear to be well-approximated by smooth nonlinear functions. We let $\mathbf{f}_j = (f_j(x_{1j}), \dots, f_j(x_{nj}))$ and $\mathbf{f}_{j,k} = (f_{j,k}(x_{1j}, x_{1k}), \dots, f_{j,k}(x_{nj}, x_{nk}))$ denote the evaluations of the main effect component f_j and the interaction component $f_{j,k}$, respectively, at the n data points. Writing \mathbf{y} for the response vector and using squared ℓ_2 -loss as the data fidelity term, the task of learning (1) can be expressed as the following optimization problem:

$$(2) \quad \min_{\substack{f_j \in \mathcal{C}_1, \forall j \\ f_{j,k} \in \mathcal{C}_2, \forall j < k}} \frac{1}{n} \left\| \mathbf{y} - \sum_{j \in [p]} \mathbf{f}_j - \sum_{j < k} \mathbf{f}_{j,k} \right\|_2^2 + \lambda_1 \left[\sum_{j \in [p]} \Omega(f_j) + \sum_{j < k} \Omega(f_{j,k}) \right],$$

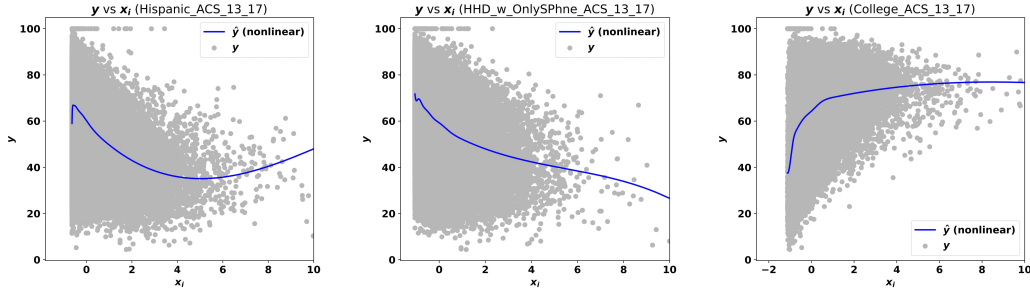


Fig 2: Panels [Left]-[Right] illustrate marginal nonparametric fits for the self-response rate output variable versus three covariates. Each marginal fit, displayed on a scatter plot with a solid blue line, clearly suggests a nonlinear relationship of the output vs the individual covariate (we note that the covariates are standardized.) The x-axis corresponds to: [Left] “Persons of Hispanic origin in the ACS”; [Middle] “Number of households that have only a smartphone and no other computing device”; [Right] “Persons 25 years and over with college degree or higher in the ACS”.

where \mathcal{C}_1 and \mathcal{C}_2 denote the sets of smooth candidate functions, Ω is a roughness penalty⁶, and λ_1 is a non-negative regularization parameter controlling the smoothness of the fit. We show in Section 2.4 that problem (2) can be written as a finite-dimensional quadratic program by using cubic splines to model each of the main and interaction effects.

2.2. *Parsimonious models via ℓ_0 -penalization.* Here we study ℓ_0 -type estimators that limit the number of components in the additive models introduced earlier.

2.2.1. *Sparse pairwise interactions.* While a significant body of work has been devoted to studying sparsity in the context of linear models, sparsity in nonlinear models has received relatively less attention. Interestingly, we observe that the notion of parsimony is linked to the model being used and changes, for example, depending on whether we use a linear interaction model of the form $\mathbb{E}(y|\mathbf{x}) = \sum_j x_j \beta_j + \sum_{j < k} x_j x_k \beta_{jk}$ or model (1) that has nonlinear components. For motivation, we consider Figure 3, which presents our findings on a 2019 US Census Bureau Planning Database dataset with 40 covariates⁷. These features include covariates used for the low-response-score (Erdman and Bates, 2014), important covariates highlighted in Appendix C of the 2019 US Census Bureau Planning Database Documentation (US Census Bureau, 2019), plus some additional covariates capturing internet penetration and urbanization. Specifically, we observe that:

- Our proposed AM approach with *nonlinear* main-effects and interactions⁸ results in a substantially more compact model than a *linear* model with interactions.
- The above nonparametric additive model leads to better test predictions compared to its linear model counterpart.
- The best (based on validation tuning with prediction error) model with linear main and interaction effects contains 37 main and 555 interaction effects. On the other hand, using nonparametric AMs, we need a total of 36 nonlinear main and interaction effects to obtain a similar test prediction performance. The nonlinear model also uses fewer covariates compared to the linear model counterpart.

⁶For example, $\Omega(f_j) = \int f_j''(x_j)^2 dx_j$ and $\Omega(f_{ij}) = \int_{x_j x_k} (\partial^2 f_{j,k} / \partial x_j^2)^2 + (\partial^2 f_{j,k} / \partial x_j \partial x_k)^2 + (\partial^2 f_{j,k} / \partial x_k^2)^2 dx_j dx_k$.

⁷These covariates were selected based on discussions with researchers at the US Census Bureau.

⁸This corresponds to an estimate available from (4). We present the model leading to the best prediction performance on the validation set – see Section 5 for details.

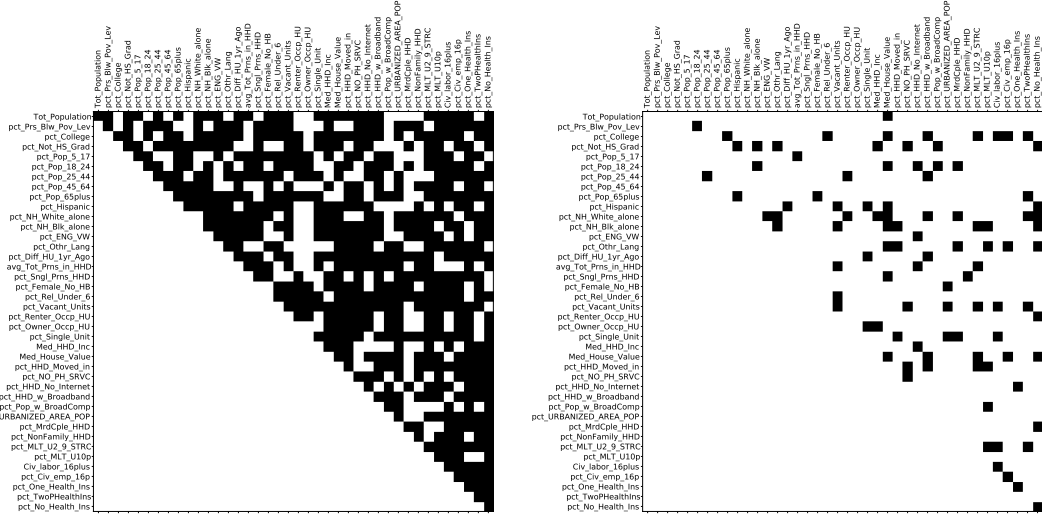


Fig 3: Sparsity pattern of the main and interaction effects presented in a $p \times p$ matrix: a black square on the diagonal indicates the presence of a main effect, and an off-diagonal black square indicates the presence of an interaction effect in the joint model. [Left] Panel illustrates the sparsity pattern of a Lasso model with main and interaction effects. There are 37 main and 555 interaction effects in the optimal model. [Right] Panel illustrates the sparsity pattern of a nonlinear AM with main and interaction effects, i.e., model (4). There are 8 main and 92 interaction effects in the optimal model. Model (4) has prediction performance similar to the Lasso model, with only 3 main and 33 interaction effects. Nonlinear models lead to much more compact and hence, easier to interpret models compared to linear models. Both models were trained on a 2019 US Census Bureau Planning Database dataset (predicting the tract-level self-response rate) with $p = 40$ covariates and 74,000 observations.

The above observations suggest that the nonlinear model with sparse interactions has advantages over its linear model counterpart for predicting survey self-response rates. As discussed in Section 5, the above findings generally carry over to the expanded dataset with a larger number of features.

To obtain an additive model with a small number of main and interaction effects, we consider an ℓ_0 -penalized modification of optimization problem (2). We write

$$(3) \quad \Omega_{\text{gr}}(f) = \sum_{j \in [p]} \Omega(f_j) + \sum_{j < k} \Omega(f_{j,k}) \quad \text{and} \quad \mathbf{f} = \sum_{j \in [p]} \mathbf{f}_j + \sum_{j < k} \mathbf{f}_{j,k},$$

to simplify the expressions, and propose an estimator that optimizes the following problem:

$$(4) \quad \min_{\substack{f_j \in \mathcal{C}_1, \forall j \\ f_{j,k} \in \mathcal{C}_2, \forall j < k}} \frac{1}{n} \|\mathbf{y} - \mathbf{f}\|_2^2 + \lambda_1 \Omega_{\text{gr}}(f) + \lambda_2 \left[\sum_{j \in [p]} \mathbb{1}[\mathbf{f}_j \neq \mathbf{0}] + \alpha \sum_{j < k} \mathbb{1}[\mathbf{f}_{j,k} \neq \mathbf{0}] \right],$$

where $\mathbb{1}[\cdot]$ is an indicator function, $\lambda_2 \in [0, \infty)$ controls the number of selected components, and $\alpha \in [1, \infty)$ controls the tradeoff between the number of main and interaction effects. We note that the finite-dimensional version of Problem (4) can be formulated as a mixed integer program (MIP) (Wolsey and Nemhauser, 1999), and hence can be solved to optimality with modern commercial solvers (for example, Gurobi, Mosek) for small/moderate scale problems. Recently, tailored nonlinear branch-and-bound techniques (Hazimeh, Mazumder and Saab, 2022) have been shown to be promising for solving large-scale instances of ℓ_0 -sparse linear regression problems. Since we intend to compute solutions to (4) for a family of tuning parameters (λ_1, λ_2) at scale, we consider high-quality approximate solutions (cf Section 2.4).

Once a good solution to (4) is available, we can employ MIP techniques to improve the solution and/or certify the quality of the solution, extending the local search techniques presented in Hazimeh and Mazumder (2020a) for ℓ_0 -sparse linear regression problems. To our knowledge, our methodological investigation of estimator (4) is novel. We refer to this model as `ELAAN-I`⁹.

While in this paper, we study a group ℓ_0 penalty in (4), one can also consider other non-convex penalty functions: for example, based on the (group) SCAD (Fan and Li, 2001) and MCP (Zhang, 2010). Exploring the statistical and computational aspects of using such penalties would be interesting to pursue and is left as future work.

Related Work. In the special case of (4), when no interactions are present, several convex relaxations of the group ℓ_0 -penalty have been studied (Ravikumar et al., 2009; Zhao and Liu, 2012; Meier, van de Geer and Bühlmann, 2009; Bühlmann and van de Geer, 2011)¹⁰. Hazimeh, Mazumder and Radchenko (2023) consider ℓ_0 -formulations for the setting without interaction effects and demonstrate the merits of using ℓ_0 -based formulations over convex relaxation-based approaches. Despite the appeal of estimator (4), computational challenges appear to be a key limiting factor in exploring this model in practice. In Section 2.4, we present a new algorithm for problem (4).

2.3. Statistical Theory. In this section, we explore statistical error bounds of our proposed estimator in the deterministic design setting. Technical details, assumptions, and proofs of the established results are provided in the supplementary material.

We write \mathcal{C}_{gr} for the space of functions $f(\mathbf{x}) = \sum_{j \in [p]} f_j(x_j) + \sum_{j < k} f_{j,k}(x_j, x_k)$, where the components belong to L_2 -Sobolev spaces, and the sparsity level of the representation is bounded. We write $G(f)$ for the number of components in the above representation:

$$G(f) = \sum_{j \in [p]} \mathbb{1}[f_j \neq \mathbf{0}] + \sum_{j < k} \mathbb{1}[f_{j,k} \neq \mathbf{0}],$$

recall the definitions of Ω_{gr} and \mathbf{f} given in (3), and let $\|\cdot\|_n$ denote the Euclidean norm divided by \sqrt{n} . We analyze the solution to optimization problem (4) with $\alpha = 1$. After a small change in notation, we focus on the following optimization problem:

$$(5) \quad \hat{f}_n = \underset{f \in \mathcal{C}_{\text{gr}}}{\operatorname{argmin}} \|\mathbf{y} - \mathbf{f}\|_n^2 + \lambda_n \Omega_{\text{gr}}(f) + \mu_n G(f),$$

where λ_n and μ_n are nonnegative tuning parameters controlling the amount of the smoothness penalty and the cardinality penalty, respectively.

We assume that the observed data follows the model $\mathbf{y} = \mathbf{f}^* + \epsilon$, where f^* is the unknown true regression function of an arbitrary form, and elements of ϵ are independent $N(0, \sigma^2)$. We refer to $\|\hat{f}_n - \mathbf{f}^*\|_n^2$ as the prediction error for estimator \hat{f}_n . We write e for the base of the natural logarithm and define $r_n = n^{-1/3}$, noting that r_n^2 is the optimal prediction error rate in the bivariate regression setting where $f^* \in \mathcal{C}_{\text{gr}}$. We say that a constant is universal if it does not depend on other parameters, such as n or p . We use the notation \lesssim to indicate that inequality \leq holds up to a positive universal multiplicative factor.

Theorem 2.1 presented below derives a general non-asymptotic oracle prediction error bound, comparing the performance of our estimator to that of sparse approximations to the true regression function. Bounds of this type have been established for sparse nonparametric

⁹`ELAAN-I` stands for `End-to-end Learning Approach for Additive spliNes with Interactions`.

¹⁰In terms of existing implementations, R package `SAM` presents specialized algorithms for a convex relaxation of (4) without interactions. `SAM` however would not run on the dataset we consider here.

AMs with main effects; however, we are not aware of similar existing bounds for nonparametric models with pairwise interactions. The existing work has focused mainly on the Lasso-based estimators, which encourage sparsity in the main-effects by penalizing the magnitudes of the functional components (see [Meier, van de Geer and Buhlmann, 2009](#); [Tan and Zhang, 2019](#), and the references therein). The use of ℓ_1 -based relaxations, in lieu of ℓ_0 -penalization, to induce sparsity in the main-effects can lead to unwanted shrinkage, which may interfere with variable selection. The approach in [Hazimeh, Mazumder and Radchenko \(2023\)](#) controls the number of main-effects directly, demonstrating the benefits of ℓ_0 -regularization both theoretically and empirically. Our analysis accounts for the interaction effects and focuses on the ℓ_0 -penalized formulation, which poses additional theoretical challenges relative to the ℓ_0 -constrained formulation. To our knowledge, the error bounds established here for sparse nonparametric AMs with pairwise interactions are novel.

The following result corresponds to the high-dimensional setting where p is large (we discuss the classical fixed p case at the end of this section), hence the stated error bound holds with high probability.

THEOREM 2.1. *Let \hat{f}_n be defined as in (5). Then, there exists a universal constant c_1 , such that if $\lambda_n \geq c_1 \sigma [r_n^2 + r_n \sqrt{\log(ep)/n}]$, then*

$$\|\hat{\mathbf{f}}_n - \mathbf{f}^*\|_n^2 + \lambda_n \Omega_{\text{gr}}(\hat{f}_n) + \mu_n G(\hat{f}_n) \lesssim \inf_{f \in \mathcal{C}_{\text{gr}}} [\|\mathbf{f} - \mathbf{f}^*\|_n^2 + \lambda_n \Omega_{\text{gr}}(f) + \mu_n G(f)] + \sigma^2 \left[r_n^2 + \frac{\log(ep)}{n} \right]$$

with probability at least $1 - 1/p$.

We note that a popular approach in the literature, even in the linear setting, has been to assume a sparse underlying model for the data. In contrast, Theorem 2.1 does not assume a ground truth sparse additive model, allowing for model misspecification and incorporating the approximation error into the bound. This feature is especially appealing for our application of interest where the ground truth is not available. The following corollary complements the general result in Theorem 2.1 by establishing a non-asymptotic prediction error bound for the proposed approach in the case where the additive model is correctly specified.

COROLLARY 1. Suppose that $f^* \in \mathcal{C}_{\text{gr}}$. There exist universal constants c_1 and c_2 , such that if $\lambda_n \geq c_1 \sigma [r_n^2 + r_n \sqrt{\log(ep)/n}]$ and $\mu_n \geq c_2 \sigma^2 [r_n^2 + \log(ep)/n] + c_2 \lambda_n \Omega_{\text{gr}}(f^*)$, then

$$(6) \quad \|\hat{\mathbf{f}}_n - \mathbf{f}^*\|_n^2 \lesssim \sigma^2 \left[r_n^2 + \frac{\log(ep)}{n} \right] + \lambda_n \Omega_{\text{gr}}(f^*) + \mu_n G(f^*) \quad \text{and} \quad G(\hat{f}_n) \leq G(f^*)$$

with probability at least $1 - 1/p$.

We note that inequality (6) yields the following prediction error bound:

$$(7) \quad \|\hat{\mathbf{f}}_n - \mathbf{f}^*\|_n^2 \lesssim \sigma^2 \left[n^{-2/3} + \frac{\log(ep)}{n} \right],$$

which holds with probability at least $1 - 1/p$ for an appropriate choice of the tuning parameters. For clarity of presentation, we do not specify the multiplicative constants in inequalities (6) and (7), focusing instead on the corresponding error rate. In contrast to the Lasso-based estimators for nonparametric AMs (e.g., [Meier, van de Geer and Buhlmann, 2009](#); [Tan and Zhang, 2019](#)), the error rate in (7) holds without imposing assumptions on the design. The accompanying sparsity bound $G(\hat{f}_n) \leq G(f^*)$ is exact, and hence stronger than the corresponding bounds for the Lasso-based estimators (e.g., [Lounici et al., 2011](#)). The latter bounds hold up to a multiplicative constant, which depends on the design and can be

significantly greater than one. When $\log(p) \lesssim n^{1/3}$, the prediction error rate in (7) matches the optimal bivariate rate of $n^{-2/3}$.

Theorem 2.1 and Corollary 1 are stated for the high-dimensional setting, where p is large. We show in the proof of Corollary 1 that in the classical asymptotic setting, where p is fixed and n tends to infinity, an appropriate choice of λ_n and μ_n leads to the optimal bivariate rate of convergence, $\|\hat{\mathbf{f}}_n - \mathbf{f}^*\|_n^2 = O_p(n^{-2/3})$, and the exact sparsity bound $G(\hat{f}_n) \leq G(f^*)$ that holds with probability tending to one.

The established error bounds also have implications for model selection. Let $\mathcal{I}(f)$ denote the index set specifying the main and interaction effects for $f \in \mathcal{C}_{\text{gr}}$. Suppose that $f^* \in \mathcal{C}_{\text{gr}}$ and the true regression model is asymptotically identifiable in the sense that $\|\mathbf{f} - \mathbf{f}^*\|_n$ is bounded away from zero for all sufficiently large n uniformly over the class $\{f \in \mathcal{C}_{\text{gr}}, G(f) \leq G(f^*), \mathcal{I}(f) \neq \mathcal{I}(f^*)\}$. If, in addition, $p = o(e^n)$ as n goes to infinity, then $\mathcal{I}(\hat{f}_n) = \mathcal{I}(f^*)$ with probability tending to one, i.e., the proposed approach is model selection consistent.

2.4. Efficient Computations at Scale. We present specialized algorithms for obtaining solutions to Problem (4). Our approach scales to the problem-size of the Census application, with $n \approx 10^5$ and $p \approx 500$, which poses formidable computational challenges due to the presence of approximately 10^5 interaction effects¹¹. To obtain good solutions at scale, we use techniques inspired by first order methods in continuous optimization (Nesterov, 2003) and a careful exploitation of the problem-structure. A high-level summary is presented below, with the details relegated to the Supplement.

State-of-the-art approaches. To appreciate the computational challenges of sparse nonlinear AMs with interactions, and nonparametric AMs in general, we provide a few examples of the problem instances that can be handled by current state-of-the-art algorithms with publicly available implementations. Current implementations based on R package SAM (Zhao and Liu, 2012), the stepwise GAM function in R package `step.gam` (which performs greedy variable selection), and Python package `pyGAM`, take on the order of days to run and/or face numerical difficulties for instances with $n \approx 10^5$ to obtain a single solution without interactions. Furthermore, `pyGAM` is unable to do automated variable selection. Wood et al. (2017) present an interesting approach for AMs that scales to large n settings (see R package `mgcv`) but doesn't appear to perform automated variable selection in the presence of a large number of features – Wood et al. (2017) report instances containing fewer than 20 pre-specified main and interaction effects. EBM (Nori et al., 2019) is a state-of-the-art computational approach for AMs, but does not allow for feature selection as all the main effects are included in the estimated model. Additionally, the variant of EBM that selects interaction effects, results in many interaction effects, leading to sub-optimal support recovery – see Sections 4 and 5 for an illustration. The GAMI-Net method (Yang, Zhang and Sudjianto, 2021) is computationally expensive. Additionally, since it uses a multi-layered NN for every interaction effect it requires $100\times$ more parameters when compared with the approaches we consider.

Algorithms for sparse nonlinear interactions: Problem (4). We represent the main and interaction effects as linear combinations of cubic spline basis functions (see the Supplement for the specific details). In particular, we let $\mathbf{f}_j = \mathbf{B}_j \boldsymbol{\beta}_j$, where $\mathbf{B}_j \in \mathbb{R}^{n \times K_j}$ is the model matrix and $\boldsymbol{\beta}_j \in \mathbb{R}^{K_j}$ is the vector of coefficients for each main effect component. Similarly, we let $\mathbf{f}_{j,k} = \mathbf{B}_{j,k} \boldsymbol{\theta}_{j,k}$, where $\mathbf{B}_{j,k} \in \mathbb{R}^{n \times K_{j,k}}$ is the model matrix and $\boldsymbol{\theta}_{j,k} \in \mathbb{R}^{K_{j,k}}$ is the vector of coefficients for each interaction effect component. Writing $\boldsymbol{\beta}$ for the vector obtained by stacking together the coefficients $\boldsymbol{\beta}_j, j \in [p]$ for the main-effects, and defining the vector $\boldsymbol{\theta}$

¹¹Note that, using 25 knots for every component, this leads to estimating around 2.5 million basis coefficients.

for the interaction effects analogously, we express the objective function in (2) as follows:

$$g_{\lambda_1}(\beta, \theta) \stackrel{\text{def}}{=} \frac{1}{n} \left\| \mathbf{y} - \left[\sum_{j \in [p]} \mathbf{B}_j \beta_j + \sum_{j < k} \mathbf{B}_{j,k} \theta_{j,k} \right] \right\|_2^2 + \lambda_1 \left[\sum_{j \in [p]} \beta_j^T \mathbf{S}_j \beta_j + \sum_{j < k} \theta_{j,k}^T \mathbf{S}_{j,k} \theta_{j,k} \right].$$

Here, $\mathbf{S}_j = \mathbf{D}_j^T \mathbf{D}_j$ and $\mathbf{S}_{j,k} = (\mathbf{D}_j^T \mathbf{D}_j) \otimes \mathbf{I}_k + \mathbf{I}_j \otimes (\mathbf{D}_k^T \mathbf{D}_k)$ are the smoothness penalty matrices for the main effects and the interaction components, respectively (further details are provided in the Supplement). For convenience, we use the same smoothness penalty λ_1 for both the main and the interaction effects, though in general they may be taken to be different. The above representation leads to the following form of the optimization problem (4):

$$(8) \quad \min_{\beta, \theta} G(\beta, \theta) \stackrel{\text{def}}{=} g_{\lambda_1}(\beta, \theta) + \lambda_2 \left[\sum_{j \in [p]} \mathbb{1}[\beta_j \neq \mathbf{0}] + \alpha \sum_{j < k} \mathbb{1}[\theta_{j,k} \neq \mathbf{0}] \right].$$

We note that the indicator functions in the above equation are applied to vectors of basis coefficients corresponding to particular main or interaction effects. Hence, for example, when $\mathbb{1}[\beta_j \neq \mathbf{0}]$ equals zero, the entire main effect \mathbf{f}_j is also zero. As mentioned earlier, (8) can be expressed as a MIP and solved for small-to-moderate scale problems using modern MIP solvers. However, given the problem-sizes of interest and the fact that we seek to compute solutions to (8) for a family of tuning parameters, we discuss faster alternatives. We note that the objective in Problem (8) is a sum of a smooth convex loss function and a discontinuous regularizer separable across the components $\{\beta_j\}$ and $\{\theta_{j,k}\}$. Motivated by the strong empirical performance of cyclical coordinate descent (CD) methods (Wright, 2015) in ℓ_0 -penalized linear regression (Hazimeh and Mazumder, 2020a), we explore block CD methods to obtain fast approximate solutions for the nonparametric setting with interactions (8). For convergence guarantees of this procedure, see Hazimeh and Mazumder (2020a) and references therein.

In our block CD method, the blocks correspond to the basis coefficients for either the main effects $\{\beta_j\}$ or the interaction effects $\{\theta_{j,k}\}$. Given an initialization $(\beta_1^{(0)}, \dots, \beta_p^{(0)}, \theta_{1,2}^{(0)}, \dots, \theta_{p-1,p}^{(0)})$, at every cycle, we sequentially sweep across the main effects and the interaction effects. In particular, if we denote the solution after t cycles by $(\beta_1^{(t)}, \dots, \beta_p^{(t)}, \theta_{1,2}^{(t)}, \dots, \theta_{p-1,p}^{(t)})$, then the block of coefficients for j -th main effect at cycle $t+1$, namely, $\beta_j^{(t+1)}$, is obtained by optimizing (8) with respect to β_j , with other variables held fixed:

$$(9) \quad \beta_j^{(t+1)} \in \underset{\beta_j \in \mathbb{R}^{K_j}}{\operatorname{argmin}} G(\beta_1^{(t+1)}, \dots, \beta_{j-1}^{(t+1)}, \beta_j, \beta_{j+1}^{(t)}, \dots, \beta_p^{(t)}, \theta_{1,2}^{(t)}, \dots, \theta_{p-1,p}^{(t)}).$$

We update $\theta_{j,k}^{(t+1)}$, containing the coefficients for the (j,k) -th interaction at cycle $t+1$, using

$$(10) \quad \theta_{j,k}^{(t+1)} \in \underset{\theta_{j,k} \in \mathbb{R}^{K_{j,k}}}{\operatorname{argmin}} G(\beta_1^{(t+1)}, \dots, \beta_p^{(t+1)}, \theta_{1,2}^{(t+1)}, \dots, \theta_{(j,k)-1}^{(t+1)}, \theta_{j,k}, \theta_{(j,k)+1}^{(t)}, \dots, \theta_{p-1,p}^{(t)}).$$

The block minimization problems (9) and (10) can be solved in closed-form as discussed in Supplement. These block CD updates need to be paired with several computational devices in the form of active set updates, cached matrix factorizations, and warm-starts, among others. We draw inspiration from similar strategies used in CD-based procedures for sparse linear regression (Hazimeh and Mazumder, 2020a; Friedman, Hastie and Tibshirani, 2010), and extend them to our problem. See Supplement Section S1.3 for more details.

CD methods have old roots in optimization dating back to the foundations of the discipline: see for example, the review paper Wright (2015). CD methods have close links with the well known Gauss-Seidel method (for solving linear/nonlinear systems of equations)—similar

methods have been extensively used in additive models (Hastie and Tibshirani, 1990), where they are referred to as *backfitting*. CD schemes (including their block variants) arising from the optimization literature can be efficiently applied to optimization problems involving sparsity constraints: such problems arise in fitting additive models with sparsity-inducing penalties (Ravikumar et al., 2009; Hastie, Tibshirani and Wainwright, 2015; Hazimeh, Mazumder and Radchenko, 2023). We note that there are other successful additive model fitting approaches, for example, smooth backfitting (Mammen, Linton and Nielsen, 1999; Mammen and Park, 2006), which have excellent theoretical properties. These works focus on the additive model setup without sparsity—extending these approaches to our setting of large-scale sparse additive models in a computationally efficient fashion is an interesting direction for future research.

3. Incorporating strong hierarchy constraints. In this section, we discuss the model with sparse interactions under strong hierarchy.

Problem (8) limits the total number of main and interaction effects and works well in our experiments (see Section 5 for the details) in terms of obtaining a sparse model with good predictive performance. In terms of variable selection properties, however, (8) can lead to the inclusion of an interaction effect, say, $\{(j, k)\}$ where at least one of the corresponding main-effects $\{j\}$ or $\{k\}$ is excluded from the model. This may be somewhat problematic from an interpretation viewpoint—it may be desirable to enforce additional constraints in (8), such as the *hierarchy constraints* (McCullagh and Nelder, 1989; Bien, Taylor and Tibshirani, 2013). In this paper, we consider the *strong hierarchy* constraint, where an interaction effect $\{(j, k)\}$ is included in the model only if both the corresponding main effects are also included. In addition to improved interpretation, strong hierarchy can reduce the *effective* number of features in the model, subsequently reducing the operational costs associated with data collection (Bien, Taylor and Tibshirani, 2013; Hazimeh and Mazumder, 2020b).

For example, based on our analysis, covariates “Males” and “Females” appear to be unnecessary for self-response prediction when the strong hierarchy constraint is imposed via model (11), while a related covariate “Households with female without spouse” remains important. In contrast, the LRS uses both “Males” and “Households with female without spouse” (Erdman and Bates, 2016) – both features appear to be important perhaps due to the use of a linear regression model. Similarly, covariates pertaining to civilian employment status across different segments/age-groups of the population, are excluded from our nonlinear AM when we learn the (sparse) main and interaction effects under strong hierarchy.

To enforce strong hierarchy into model (8), we consider the following estimator:

$$(11a) \quad \min_{\beta, \theta} \quad g_{\lambda_1}(\beta, \theta) + \lambda_2 \left(\sum_{j \in [p]} \mathbb{1}[\beta_j \neq 0] + \alpha \sum_{j < k} \mathbb{1}[\theta_{j,k} \neq 0] \right)$$

$$(11b) \quad \text{s.t.} \quad \theta_{j,k} \neq 0 \implies \beta_j \neq 0 \ \& \ \beta_k \neq 0 \quad \forall j < k, j \in [p], k \in [p].$$

We note that (11) differs from (8) in the additional strong hierarchy constraint appearing in (11b). By using binary variables to model sparsity in the main/interaction effects and to encode the hierarchy constraint (11b), Problem (11) can be expressed as the following MIP:

$$(12a) \quad \min_{\beta, \theta, z} \quad g_{\lambda_1}(\beta, \theta) + \lambda_2 \left(\sum_{j \in [p]} z_j + \alpha \sum_{j < k} z_{j,k} \right)$$

$$(12b) \quad \text{s.t.} \quad z_j, z_{j,k} \in \{0, 1\}, \quad \|\beta_j\|_2^2 \leq M z_j, \quad \|\theta_{j,k}\|_2^2 \leq M z_{j,k} \quad \forall j < k, j, k \in [p],$$

$$(12c) \quad z_{j,k} \leq z_j, \quad z_{j,k} \leq z_k, \quad \forall j < k,$$

where the BigM parameter M is a sufficiently large finite constant such that an optimal solution to (12) satisfies $\max_j \|\beta_j\|_2^2 \leq M$ and $\max_{j,k} \|\theta_{j,k}\|_2^2 \leq M$. Binary variable z_j (and $z_{j,k}$) indicates whether the corresponding main effect β_j (respectively, interaction effect $\theta_{j,k}$) is zero or not; the constraint appearing in (12c) enforces the hierarchy constraint in (11b).

To our knowledge, ours is the first work to study estimator (12). The methodology presented here is of independent interest in the context of structured nonparametric learning with interactions. We refer to this model as ELAAN-H¹². In Section S3 of the Supplement, we propose algorithms to obtain good solutions to Problem (12).

Related Work. Methodology for strong hierarchy in linear models has been studied in the statistics/machine learning literature (Bien, Taylor and Tibshirani, 2013; Lim and Hastie, 2015; Yan and Bien, 2017; Hazimeh and Mazumder, 2020b) – these works focus on the linear model setting, a special case of the nonlinear setting we consider here. Radchenko and James (2010) consider hierarchy constraints in the nonparametric setting via convex optimization schemes. To our knowledge, current techniques are unable to scale to the functional learning instances we consider in our paper.

As mentioned earlier, the EBM approach (Nori et al., 2019) does not support hierarchy constraints. GAMI-Net (Yang, Zhang and Sudjianto, 2021) follows a two-stage approach to fit nonparametric additive models with sparse (weak) hierarchical interactions. GAMI-Net performs a screening step after estimating the main effects with neural-network blocks and only consider interaction effects that satisfy the weak hierarchy principle amongst the screened main effect – an interaction effect can appear in the model if one of the main effects is in the model. As mentioned earlier, GAMI-Net is not based on an optimization procedure; and can be computationally much more expensive than our estimators.

4. Simulations. In this section we study the empirical performance (estimation and prediction) of the ELAAN-I and ELAAN-H estimators on synthetic datasets.

4.1. Sparse additive model with interactions. Motivated by Li, Lue and Chen (2000), we consider a problem with $p = 10$ features where the true underlying model is additive in a small number of main and interaction effects:

$$(13) \quad \begin{aligned} f^*(\mathbf{x}) = & g_1(x_1) + g_2(x_2) + g_3(x_3) + g_4(x_4) \\ & + g_1(x_3x_4) + g_2\left(\frac{x_1 + x_3}{2}\right) + g_3(x_1x_2), \end{aligned}$$

where functions $g_1(t) = t$, $g_2(t) = (2t - 1)^2$, $g_3(t) = \frac{\sin(2\pi t)}{2 - \sin(2\pi t)}$, and $g_4(t) = 0.1\sin(2\pi t) + 0.2\cos(2\pi t) + 0.3\sin^2(2\pi t) + 0.4\cos^3(2\pi t) + 0.5\sin^3(2\pi t)$ are defined on $[0, 1]$. Note that the covariates x_5, \dots, x_{10} do not contribute to the response. Each of the covariates x_1, \dots, x_{10} are independently drawn from the uniform distribution $\mathcal{U}(0, 1)$. We generate the responses as $y = f^*(\mathbf{x}) + \epsilon$, where the errors ϵ are drawn from a Gaussian distribution $\mathcal{N}(0, 0.2546^2)$.

We measure prediction accuracy using the integrated squared error, $\text{ISE} = \mathbb{E}_{\mathbf{x}}[(\hat{f}(\mathbf{x}) - f^*(\mathbf{x}))^2]$, estimated by Monte Carlo integration using 10,000 test observations from the same distribution as the training ones, following the procedure in Li, Lue and Chen (2000). We vary the number of training observations from 100 to 400 and use 100 replications for each simulation setting. We compare our estimators to well-known benchmarks EBM (Nori et al., 2019), GAMI-Net (Yang, Zhang and Sudjianto, 2021), COSSO (Lin and Zhang, 2006), and MARS¹³ (Friedman, 1991).

¹²ELAAN-H stands for End-to-end Learning Approach for Additive spliNes with Hierarchy.

¹³MARS is a stepwise forward/backward procedure for building functional ANOVA models.

Table 1 presents the average test ISE and their standard errors (based on the replications). The tuning parameters for ELAAN-I, ELAAN-H, EBM and GAMI-Net are selected via 5-fold cross-validation. The results for MARS and COSSO are taken from Table 6 in Li, Lue and Chen (2000). Table 1 demonstrates that both of our estimators, ELAAN-I and ELAAN-H, outperform the competitors across the entire range of training set sizes under consideration. Due to space constraints, additional simulations comparing our approach to EBM and with similar conclusions are provided in the Supplement Section S4.2.2.

Next, we study the support recovery performances of ELAAN-I, ELAAN-H, EBM and GAMI-Net. We evaluate models using discrepancy between the true and estimated support and separately report the average F1-score for the main and the interaction effects. The support recovery metrics are shown in Table 2. We observe that, overall, both ELAAN-I and ELAAN-H appear to outperform EBM and GAMI-Net in terms of the F1-score. Moreover, ELAAN-H is seen to be the best-performing method across all the simulation settings. In summary, our approaches work quite well in terms of variable selection.

Table 3 presents additional variable selection details of the two best-performing approaches: ELAAN-I and ELAAN-H. For each true main and interaction effect, we report the relative frequency of their appearance in the estimated support across all replications. The results in Tables 2 and 3

suggest that ELAAN-H outperforms ELAAN-I in terms of the variable selection when the true model is hierarchical. In practice, when we do not know if the underlying truth obeys strong hierarchy, ELAAN-H tends to result in more compact models, as we demonstrate in the Census application in Section 5.

4.2. Large-scale setting with correlated features. Next, we evaluate our proposed methods on large-scale synthetic data with $p = 500$ correlated features. We draw (x_1, \dots, x_p) from a multivariate normal distribution $\mathcal{N}(0, \Sigma)$, where $\Sigma_{ij} = \sigma^{|i-j|}$ with $\sigma \in [0, 1]$. We generate the responses as $y = f^*(\mathbf{x}) + \epsilon$, where $\epsilon \sim \mathcal{N}(0, 0.25)$ and

$$f^*(\mathbf{x}) = h_1(x_{26}) + h_2(x_{76}) + h_3(x_{126}) + h_4(x_{176}) + h_5(x_{226}) + h_6(x_{276}) \\ + h_1(x_{326}) + h_2(x_{376}) + h_3(x_{426}) + h_4(x_{476})$$

Table 1: Integrated Squared Errors for ELAAN-I, ELAAN-H, MARS, COSSO, EBM and GAMI-Net.

N_{train}				
Model	100	200	400	
MARS	0.239 \pm 0.008	0.109 \pm 0.003	0.084 \pm 0.001	
COSSO	0.378 \pm 0.005	0.094 \pm 0.004	0.043 \pm 0.001	
EBM	0.274 \pm 0.004	0.170 \pm 0.002	0.100 \pm 0.001	
GAMI-Net	0.281 \pm 0.007	0.114 \pm 0.004	0.063 \pm 0.003	
ELAAN-I	0.220 \pm 0.013	0.077 \pm 0.002	0.035 \pm 0.001	
ELAAN-H	0.180 \pm 0.008	0.081 \pm 0.004	0.038 \pm 0.001	

Table 2: Support recovery metric (F1-score) for the main effects and the interaction effects.

N_{train}	Model	F1 (main)	F1 (Interactions)
100	EBM	57.14 \pm 0.00	51.47 \pm 1.89
	GAMI-Net	61.77 \pm 0.79	22.31 \pm 1.27
	ELAAN-I	85.35 \pm 1.24	40.30 \pm 2.78
	ELAAN-H	93.46 \pm 1.14	66.61 \pm 2.45
200	EBM	57.14 \pm 0.00	70.43 \pm 2.07
	GAMI-Net	59.23 \pm 0.41	33.01 \pm 1.51
	ELAAN-I	90.55 \pm 1.02	74.83 \pm 1.58
	ELAAN-H	98.52 \pm 0.43	82.43 \pm 1.38
400	EBM	57.14 \pm 0.00	83.47 \pm 1.86
	GAMI-Net	58.11 \pm 0.30	39.24 \pm 2.16
	ELAAN-I	97.43 \pm 0.62	87.34 \pm 1.17
	ELAAN-H	99.31 \pm 0.41	90.17 \pm 1.23

Table 3: Relative frequency of the true main and interaction effects appearing in the ELAAN-I and ELAAN-H models.

N_{train}								
Components	100		200		400		1000	
	ELAAN-I	ELAAN-H	ELAAN-I	ELAAN-H	ELAAN-I	ELAAN-H	ELAAN-I	ELAAN-H
$x^{(1)}$	87%	97%	79%	100%	89%	100%	90%	100%
$x^{(2)}$	67%	93%	88%	100%	99%	100%	100%	100%
$x^{(3)}$	100%	95%	100%	98%	100%	100%	100%	100%
$x^{(4)}$	99%	99%	100%	99%	100%	99%	100%	100%
$[x^{(1)}, x^{(2)}]$	69%	100%	100%	100%	100%	100%	100%	100%
$[x^{(1)}, x^{(3)}]$	18%	100%	74%	94%	97%	99%	100%	100%
$[x^{(3)}, x^{(4)}]$	0%	96%	14%	33%	42%	59%	99%	96%

$$\begin{aligned}
& + h_1(x_{26})h_2(x_{76}) + h_1(x_{26})h_3(x_{126}) + h_4(0.5(x_{126} + x_{176})) + h_4(x_{176})h_5(x_{226}) \\
& + h_4(x_{176})h_6(x_{276}) + h_5(x_{326}x_{376}) + h_6(x_{426}x_{476}) + h_4(x_{276}x_{476}),
\end{aligned}$$

with $h_1(t) = 0.5t$, $h_2(t) = 1.25\sin(t)$, $h_3(t) = 0.3\exp(t)$, $h_4(t) = 0.5t^2$, $h_5(t) = 0.9\cos(t)$, and $h_6(t) = 1/(1 + \exp(-t))$.

We produce 10,000 training observations and evaluate the prediction performance as before, using ISE on a test set of size 10,000. We compare our estimators to EBM (Nori et al., 2019) and GAMI-Net (Yang, Zhang and Sudjianto, 2021). Table 4 presents the average prediction errors and support recovery metrics over 25 simulation replications, along with the corresponding standard errors. The tuning procedure for ELAAN-I, ELAAN-H, EBM and GAMI-Net is described in the Supplement. Table 4 demonstrates that our proposed models consistently and significantly outperform the competitors, exhibiting a 7-11 fold reduction in the prediction error.

Table 4: Integrated Squared Errors and support recovery metrics for EBM, GAMI-Net, ELAAN-I and ELAAN-H on large-scale synthetic data with different correlation strengths (σ).

σ	Model	Prediction Error	Support Recovery		
		ISE ($\times 10^{-2}$)	F1 (features)	F1 (main)	F1 (Interactions)
0.1	EBM	379.1 \pm 5.3	3.92 \pm 0.00	3.92 \pm 0.00	26.41 \pm 3.26
	GAMI-Net	81.8 \pm 7.3	56.57 \pm 4.10	92.25 \pm 2.44	11.65 \pm 1.78
	ELAAN-I	8.9 \pm 0.9	98.95 \pm 0.69	67.75 \pm 4.77	95.17 \pm 1.17
	ELAAN-H	7.4 \pm 0.8	98.72 \pm 0.59	98.72 \pm 0.59	93.78 \pm 1.65
0.3	EBM	381.4 \pm 4.24	3.92 \pm 0.00	3.92 \pm 0.00	28.26 \pm 3.07
	GAMI-Net	83.2 \pm 7.2	55.20 \pm 4.52	94.20 \pm 2.04	12.00 \pm 2.29
	ELAAN-I	11.4 \pm 1.6	99.24 \pm 0.35	65.90 \pm 5.07	95.10 \pm 1.08
	ELAAN-H	10.0 \pm 1.6	98.16 \pm 1.80	98.16 \pm 1.80	93.48 \pm 2.41
0.5	EBM	386.4 \pm 5.9	3.92 \pm 0.00	3.92 \pm 0.00	26.00 \pm 3.40
	GAMI-Net	77.9 \pm 6.2	58.06 \pm 4.15	93.92 \pm 2.11	13.24 \pm 2.04
	ELAAN-I	12.4 \pm 1.7	100.00 \pm 0.00	60.04 \pm 5.75	95.25 \pm 1.00
	ELAAN-H	10.6 \pm 1.8	98.87 \pm 0.54	98.87 \pm 0.54	94.32 \pm 1.05
0.7	EBM	375.7 \pm 3.3	3.92 \pm 0.00	3.92 \pm 0.00	17.20 \pm 2.06
	GAMI-Net	78.4 \pm 7.0	62.42 \pm 4.18	94.80 \pm 1.97	14.87 \pm 2.67
	ELAAN-I	9.3 \pm 0.8	99.43 \pm 0.31	77.38 \pm 4.71	97.12 \pm 0.98
	ELAAN-H	10.6 \pm 1.8	97.57 \pm 0.68	97.57 \pm 0.68	91.31 \pm 1.52

5. Case study: Predicting the Census Survey Self-Response Rate. We now present our findings on the Census application. As mentioned in Section 1, obtaining interpretable models with good predictive capabilities is important in this application – such models can inform the planning of outreach campaigns and guide stakeholders in deciding the allocation of spending for different communications channels (for example, TV, radio, digital), advertising messages with appropriately tailored content, and the timing of spending during the campaigns (Kulzick et al., 2019). Due to their opaque nature, predictive models that topped the nationwide competition were not actionable for this application. On the other hand, the linear models that drive the LRS have limited predictive power. We explore how our proposed approach balances simplicity and good prediction performance.

The data we use for this study is publicly available in the US Census Planning Database, which provides a range of demographic, socioeconomic, housing, and Census operational data (US Census Bureau, 2019). The data in the Planning Database includes covariates from the 2010 Census and the 2013-2017 American Community Survey (ACS), aggregated at both the Census tract level and the block level. We use tract-level data, with approximately 74,000 observations and 500 covariates. The response is the ACS self-response rate. We exclude the following covariates from our model: spatial covariates (“State”, “County”, “Tract”, “Flag”, “AIAN Land”) and variables that serve as a proxy to the response (for example, “Low response score”, “Number of housing units that returned first forms”, “Replacement forms” or “Bilingual forms” in Census 2010). We also remove the margin of error variables corresponding to the ACS. After excluding these variables, we are left with $p = 295$ covariates¹⁴.

¹⁴To clarify, the results presented in this section are based on these 295 features, though our approach scales to $p = 500$ features.

5.1. Experimental setup. We randomly split the data into 58K for training, 7.2K for validation (used for selecting tuning parameters), and 7.2K observations for testing. We repeat this procedure 20 times with different random splits of the data and report the average numbers on the test sets. The features were standardized to have zero mean and unit variances. We use the squared ℓ_2 loss for training and evaluate the performance of the models in terms of root mean square (RMSE). We also study the variables selected by our algorithm: for example, the number of features retained and the associated interpretations they offer.

As noted in [Erdman and Bates \(2016\)](#), the current approach for predicting the self-response rates—i.e., the LRS—is based on a linear regression model with around 25 *hand-selected* features. Erdman and Bates also use tailored variable transformations on some features to incorporate nonlinear effects. When the number of features, both main and pairwise interaction effects, increase, it is desirable to have an automated procedure such as the one we propose. As we use nonparametric models, which seek to learn nonlinearities in the main and interaction effects, manual feature engineering may not be necessary.

Benchmark Methods. We evaluate and compare our models against existing linear and nonparametric approaches. We consider the following linear models with main effects only (i.e., without interactions): (i) Ridge regression; (ii) Lasso regression ([Hastie, Tibshirani and Wainwright, 2015](#)); (iii) ℓ_0 -penalized regression with additional ridge regularization (denoted as $\ell_0 - \ell_2$), implemented via `L0Learn` ([Hazimeh and Mazumder, 2020a](#)). In addition, we consider the following linear models with interaction effects: (iv) Lasso with main effects and all pairwise linear interactions, (v) `hierScale`: a convex optimization framework for learning sparse main-effects and interactions under a strong hierarchy constraint ([Hazimeh and Mazumder, 2020b](#)). For (i), (ii), and (iv), we use Python’s `scikit-learn` library ([Pedregosa et al., 2011](#)).

In addition to the competing methods discussed above based on linear models, we consider nonparametric additive models with/without interactions. For AMs with main effects only, we compare with (vi) Additive Models with Lasso-based selection, which we fit using Python’s `scikit-learn` library ([Pedregosa et al., 2011](#)). For additive models with interactions, we consider (vii) EBM: A boosting approach that uses trees for main and interaction effects ([Nori et al., 2019](#)). (viii) GAMI-Net: a neural network-based additive model with structured interactions ([Yang, Zhang and Sudjianto, 2021](#)). For EBM, we tune the learning rate in the range $[10^{-4}, 10^{-1}]$ and the number of interactions in the range $[10, 500]$ for 1000 trials. For GAMI-Net, we run the model once with a 200 batch-size, 0.0001 learning rate, 500 interaction effects, 500 epochs (for each stage) and 0.0001 loss threshold. We note that GAMI-Net took 3 days to complete using a machine with 8-CPU and 128GB RAM.

In addition to the linear and additive model benchmarks mentioned above, we also compare with state-of-the-art black-box machine learning methods such as (ix) Gradient boosted decision trees (GBDT) from XGBoost ([Chen and Guestrin, 2016](#)); and (x) Neural networks: multilayer perceptron (MLP). The tuning parameters in both the models (ix) and (x) are selected using the Python hyperparameter optimization package `hyperopt` ([Bergstra et al., 2015](#)). GBDT is tuned with respect to the maximum depth $[1 - 10]$, number of estimators $[10 - 200]$, learning rate $[10^{-4}, 1]$. Neural networks are tuned with respect to the number of dense layers $\{2, 3, 4, 5, 6, 7\}$, number of hidden units $\{64, 128, 256, 512\}$, dropout rate $\{0.1, 0.2, 0.3\}$, learning rates $\{0.1, 0.01, 0.001, 0.0001\}$ for Adam optimizer ([Kingma and Ba, 2015](#)), batch sizes $\{64, 128\}$ and epochs $\{25, 50, 75, 100\}$. The number of tuning parameters for all the nonparametric models is capped at 1000.

Proposed Models. Among our proposed estimators, we consider: (a) ELAAN: ℓ_0 -penalized AMs with nonlinear main effects. We also consider the following AMs containing both main and pairwise interaction effects: (b) ELAAN-I: ℓ_0 -penalized AMs with both main and interaction effects, i.e., estimator (8); and (c) ELAAN-H: sparse hierarchical interactions, i.e., estimator (12).

TABLE 5

Comparisons of our methods with several benchmark models as discussed in the text. We display the average test RMSE for the different models, along with the corresponding number of covariates, and number of effects (main and interactions). Best metrics are highlighted in bold. Numbers after \pm provide the standard errors. Asterisk(*) indicates statistical significance (p-value<0.05) over the best existing model, using a one-sided paired t-test. Models (ix), (x) are black-box models using higher order interactions, hence #Main and #Interactions are left as ‘-’ (dash).

Type	Model	RMSE	#Covariates	#Main	#Interactions
Linear Models (LM)	(i) Ridge	6.750 \pm 0.013	295 \pm 0	295 \pm 0	-
	(ii) Lasso	6.741 \pm 0.013	226 \pm 7	226 \pm 7	-
	(iii) L0Learn ($\ell_0 - \ell_2$)	6.752 \pm 0.012	145 \pm 3	145 \pm 3	-
Linear Models with Interactions (LMI)	(iv) LMI with Lasso	6.514 \pm 0.019	262 \pm 2	75 \pm 2	1592 \pm 79
	(v) LMI with Strong Hierarchy (hierScale)	6.528 \pm 0.018	276 \pm 2	276 \pm 3	4107 \pm 179
Additive Models (AM)	(vi) AM with Lasso	6.548 \pm 0.015	285 \pm 1	285 \pm 1	-
	(a) ELAAN	6.566 \pm 0.014	184 \pm 11	184 \pm 11	-
Additive Models with Interactions (AMI)	(vii) EBM	6.475 \pm 0.014	295 \pm 0	295 \pm 0	492 \pm 1
	(viii) GAMI-Net	6.573 \pm 0.015	246 \pm 5	224 \pm 4	150 \pm 26
	(b) ELAAN-I	*6.442 \pm 0.019	154 \pm 8	33 \pm 5	201 \pm 19
	(c) ELAAN-H	*6.425 \pm 0.019	133 \pm 6	133 \pm 6	255 \pm 13
Nonparametric (Non-interpretable)	(ix) GBDT	6.481 \pm 0.016	278 \pm 0	-	-
	(x) Neural Networks (MLP)	6.505 \pm 0.016	295 \pm 0	-	-

All our algorithms for estimators (a)–(c) are implemented in Python. We use cubic B-splines with 10 knots for the main effects. For the interaction effects, we use tensor spline bases of degree 3 with 5 knots in each coordinate, leading to a total of $5 \times 5 = 25$ knots¹⁵. Because the problem at hand has 295 covariates and 43,365 possible pairwise interactions, we need to be careful with implementation aspects while generating spline-transformed representations for all the interaction effects, which can be memory intensive.

For ELAAN and ELAAN-I we perform a tuning procedure with warm-starts over a 2D grid of parameters (λ_1, λ_2) – for details, see Supplement Section S1.4.3. For both ELAAN-I and ELAAN-H, we set $\alpha = 1$ so that the main and the interaction effects have the same ℓ_0 -penalty parameter. For ELAAN-H, we fix the smoothing parameter λ_1 to the optimal value available from ELAAN-I. Parameter λ_2 (as well as parameter τ defined in Supplement Section S3) is chosen based on validation tuning. For all our methods (ELAAN, ELAAN-I, ELAAN-H), we cap the number of tuning-parameter values at 1000.

5.2. Comparing methods: prediction, sparsity and model structure. We discuss the performance of different estimators in terms of prediction error and model parsimony.

Additive models vs black-box ML methods. Table 5 reports the prediction errors (RMSE) on the test-set along with the number of nonzero features in the model. Importantly, we observe that the test performances of AMs with sparse interactions (both with and without the hierarchy constraints) are better than that of the best black box predictive ML models (ix), (x) that are based on GBDT, Neural Networks. Our model ELAAN-H delivers the best RMSE value and is closely followed by ELAAN-I.

ELAAN-I/ELAAN-H vs prior art for AMs with sparse interactions.

Among the methods we compared, EBM and GAMI-Net were the only methods that could compute AMs with sparse interactions for the Census dataset. Interestingly, the test performances of both ELAAN-I and ELAAN-H are better than EBM and GAMI-Net. Interpretability (i.e., model sparsity and/or hierarchy) is another key factor differentiating the leading prediction methods. Our models select a smaller number of additive components than EBM and GAMI-Net. For example, ELAAN-I selects a total of 234 additive components. In contrast, EBM and GAMI-Net select 787 and 374 additive components, respectively. Similarly,

¹⁵We study the effect of number of knots on out-of-sample generalization on synthetic data (see Supplement Section S4.2.1).

we also observe that our models are substantially more compact in terms of the number of selected covariates by a factor of (approximately) two.

While Table 5 presents a summary of the best models chosen based on the validation set prediction performance, a practitioner may also find it useful to study a family of models prioritizing models with fewer features (perhaps at the cost of a marginal deterioration in predictive performance) – see Section 5.3 for further discussion.

We briefly discuss computation times for different methods. EBM takes around one hour to fit a model with 500 pairwise interactions (for a single tuning parameter). Computing a GAMI-Net solution (for one tuning parameter corresponding to 500 interaction effects) takes around 3 days using 8 CPUs and 10 hours using a single V100 Tesla GPU. In contrast, our approaches are much faster: ELAAN-I takes on average 1.8 mins to compute a solution for a fixed tuning parameter¹⁶. When ELAAN-H is run on a reduced subset of 800 pairwise interactions, it takes 1.5 hours to compute a path of 100 solutions. These numbers are reported on an 8-CPU 128GB RAM device.

Nonlinear models vs linear models. Table 5 suggests that nonlinear/nonparametric models have better predictive performance than their linear counterparts. Also, linear models with sparse main and interaction-effects appear to have an edge over sparse linear models without interactions. Another appealing aspect of sparse nonparametric AMs compared to linear models, is in model parsimony – we alluded to this aspect in Figure 3 while using a reduced number of features. The number of nonzero effects is significantly lower for the nonlinear AMs. For example, ℓ_0 -sparse nonparametric AMs with no interactions (i.e., ELAAN) can achieve the same level of predictive performance as its linear model counterpart (i.e., Model (iii)) with significantly fewer covariates: 40 versus 145. Similarly, if we compare `hierScale` (i.e., linear main and interaction effects with strong hierarchical restrictions) to its nonparametric counterpart i.e., ELAAN-H, the number of main effects (and also, covariates) reduces from 276 to 133, and the number of interaction effects reduces from 4,107 to 255. Interestingly, all the covariates selected by the nonparametric AMs with interaction models (with/without strong hierarchy) are contained in the set of covariates selected by the sparse linear models with both main and interaction effects.

Additive nonlinear models: interactions vs no interactions. Table 5 shows that ELAAN (AMs with no interactions) has more covariates than AMs with interactions, both ELAAN-I and ELAAN-H. By including interactions that obey the hierarchy principle, we select a smaller number of covariates: ELAAN-I has 154 covariates vs ELAAN-H has 133. The difference between ELAAN vs ELAAN-I is possibly because many nonlinear main effects attempt to explain the nonlinear interaction effects. This reduction points to the redundancy of some of the covariates when interaction effects are directly included in the model. The prediction performance of nonlinear AMs seems to improve significantly when pairwise interactions are included in the model.

Hierarchy vs no hierarchy. We observe that ELAAN-H, i.e., additive model with hierarchical interactions, achieves the best out-of-sample RMSE – this improves over ELAAN-I (interactions with no hierarchy). The improvement is statistically significant based on a paired t-test. We observe that ELAAN-I selects fewer effects (33 Main + 201 Interactions) when compared to ELAAN-H (133 Main + 255 Interactions). On the other hand, ELAAN-H obeys the hierarchy constraint and selects fewer covariates than ELAAN-I – this can aid in interpretability and be easier to operationalize from a practical standpoint.

Insights from visualizations. As illustrated by Figure 2, which displays some marginal nonlinear fits, an appealing aspect of nonlinear AMs is that they naturally allow the practitioner

¹⁶We use warm-start continuation across λ_2 -values for a fixed λ_1 : it takes approximately 3 hours to compute 100 solutions where the maximum number of pairwise interactions is 500.

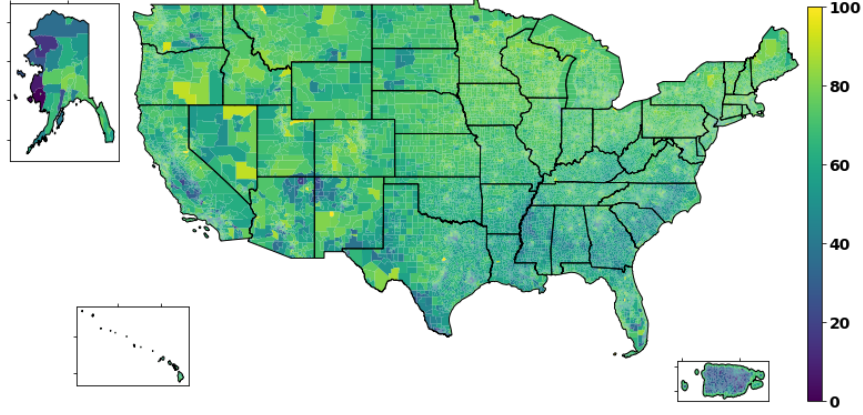


Fig 4: Predicted ACS self-response rates for all tracts in the United States.

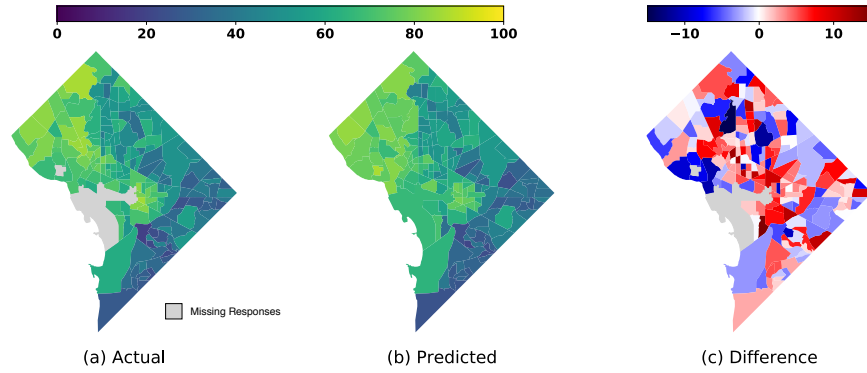


Fig 5: ACS self-response rates for all tracts in the District of Columbia. a) Actual ACS self-response rates. b) Predicted ACS self-response rates for AMs with interactions (8). c) Difference between the actual and predicted self-response rate: difference = actual - predicted.

to gather insights into the associations between the response and a feature of interest, for example, by exploring the map $x_j \mapsto f_j(x_j)$. Similarly, the map $(x_j, x_k) \mapsto f_{j,k}(x_j, x_k)$ would shed light into how the interaction of (x_j, x_k) influences the output. Such interpretations are a by-product of our additive model framework; and may not be readily available via black-box ML methods such as Neural Networks and GBDT—see also [Lou et al. \(2013\)](#) for related discussions advocating for the interpretability of AMs. These association plots, for example, can help stakeholders identify promising factors and patterns influencing self-response scores potentially informing policy decisions (e.g, targeted investments and optimizing operational costs).

To obtain a finer understanding of the performance of our models, we use visualization tools inspired by earlier works from the US Census Bureau ([US Census Bureau, 2017](#); [Kulzick et al., 2019](#)). Figure 4 illustrates the tract self-response rates predicted by ELAAN-I i.e., model (8) on a map of the United States. Different from Figure 1, which shows actual data with missing values for some of the tracts¹⁷, Figure 4 provides predicted self-response rates

¹⁷Some responses are deliberately suppressed by the US Census Bureau for privacy considerations, to limit the disclosure of information about individual respondents and to reduce the number of estimates with unacceptable levels of statistical reliability ([US Census Bureau, 2016](#))

for all tracts based on our proposed model. Predictive models in general and our models in particular, allow us to forecast the response rates for tracts where gathered data is incomplete. It is worth noting that our regression-based models may be preferable over commonly used nearest neighbor type methods: the latter models do not generally offer insights into factors associated with high/low response rates. Nearest neighbor based methods may also be ill-posed for isolated regions such as Alaska, Hawaii and Puerto Rico, each having at least 10% of their tracts censored.

Figure 5 displays, side by side, the actual and the predicted self-response rates for the tracts in Washington DC, as well as the corresponding differences. Both the actual and the predicted rates are higher than average in most parts of the Northwest and a portion of the Northeast DC, and lower in the Southeast and most of the Northeast DC.

Figure 6 shows how the sorting of the Census tracts into quintiles (US Census Bureau, 2017; Kulzick et al., 2019) of the actual self-response rates compares with the corresponding sorting of the predictions made by: the Lasso (we use an ℓ_1 -penalized linear model with main effects and no interactions), and ELAAN-I. For example, the top panel in Figure 6 shows that among the tracts in the first quintile of the actual self-response rates, 85.1% are correctly predicted by ELAAN-I to fall in the first quintile. The corresponding proportion for Lasso is 84.4%. The same panel shows that among the tracts in the first quintile of the actual self-response rates, 14.1% are incorrectly predicted to fall in the second quintile; this proportion is smaller than the one for the Lasso (14.7%). Similarly, in the second quintile of the actual self-response rates, a higher proportion (58.4%) is correctly identified by ELAAN-I to be in the second quintile; this is again an improvement over the 56.6% for the Lasso regression model. For all 5 quintiles of the actual self-response rates, ELAAN-I identifies a higher proportion to be in the correct quintile than Lasso, suggesting that our approach has an edge over the Lasso.

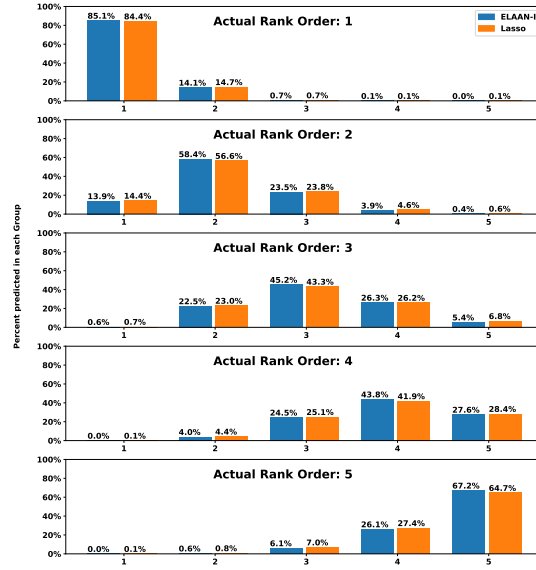


Fig 6: Comparison of quintile groups based on Lasso (linear model) (US Census Bureau, 2017; Kulzick et al., 2019) and our proposed ELAAN-I.

5.3. Interpreting important features. We now illustrate how our methodology can guide the practitioner in obtaining a set of features and deriving associated actionable insights into the factors contributing towards low response-rates in surveys. An important aspect of our regularized learning framework is that it provides an automated scheme to identify a collection of models, balancing out the complexity of the model and data-fidelity. To see this, Figure 7[left panel] plots the number of main and interaction effects against the associated prediction error for model (8). The plot illustrates that by trading off a little in the predictive performance (in terms of RMSE, which is shown by the red dashed line), we can limit the number of effects at any level, as desired by the practitioner who intends to obtain a more parsimonious representation of the factors impacting survey response rates. Specifically, if we would like to limit the number of main effects to under 20, Figure 7(b) shows the top 19 main effects in the order they enter the model along the regularization path. The definitions

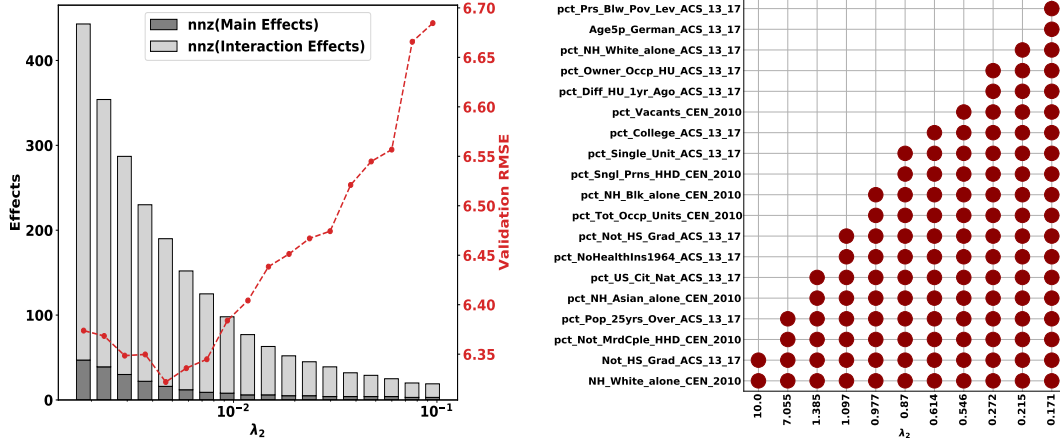


Fig 7: Estimates available from our model *ELAAN-I* i.e., model (8): ℓ_0 -sparse AMs with main effects and interactions. [Left] number of nonzero effects vs the corresponding RMSE. [Right] Variables corresponding to main effects selected by the model along the regularization path. For visualization purposes, we focus on the top 19 main effects.

of the variables in Figure 7(b) are provided in the Supplement. Our investigation reveals that most (though not all) of these variables also appear in the models reported in prior studies by the Census Bureau – see for example [Erdman and Bates \(2016\)](#) and [Kulzick et al. \(2019\)](#). Interestingly, some of the features discovered by our framework can be interpreted in the context of clusters defined in [Bates and Mulry \(2011\)](#) or mindset solutions in [Kulzick et al. \(2019\)](#), as discussed below.

Using cluster analysis on the 12 covariates from the HTC score, [Bates and Mulry \(2011\)](#) categorize the tracts into eight distinct clusters: All Around Average I and II, Economically Disadvantaged I and II, Ethnic Enclave I and II, Single Unattached Mobiles, and Advantaged Homeowners. From the cluster analysis in [Bates and Mulry \(2011\)](#), we see that the reported clusters have a wide variation in response rate (the response rate is not used to identify the clusters). Each cluster has some key characteristics (pertaining to a subset of variables) that seem to drive the response rate. From the description of these clusters in [Bates and Mulry \(2011\)](#), we see that the covariates automatically discovered by our framework, as listed in Figure 7[right panel], broadly cover the important characteristics upon which the clusters are based. For example, there is high variability across clusters with respect to the occupancy rate and home ownership status, which are captured by covariates “Owner occupied housing units” and “Total occupied units”. Racial diversity also appears to play a role in cluster formation – in particular, the covariates related to ethnic groups characterize the Ethnic Enclave clusters. Similarly, covariates related to poverty, for example, “Persons below poverty line”, lack of education (“No high school diploma”), and lack of health insurance (“No health insurance”), determine the Economically Disadvantaged clusters. Covariates related to high mobility, for example, “Different housing unit in prior year”, high education (“College or higher degree holders”), marital status (“Single person households”), and nonspousal occupants (“Unmarried couples”), characterize the Single Unattached Mobiles cluster.

The above discussion suggests that there may be important interaction effects within the variable groups that characterize each cluster. We observe that our AMs with interactions model (8) automatically selects many of these effects. For instance, our model recovers several interaction effects between important covariates characterizing the Economically Disadvantaged I cluster. [Bates and Mulry \(2011\)](#) notes that this cluster has high percentages of

people in poverty, people receiving public assistance, and adults without a high school education. Our model identifies an interaction effect between “No high school graduation” and “No health insurance”. The same cluster also has a large African American population and above average number of children under 18. Our model potentially captures this characteristic by selecting an interaction effect between “Non-Hispanic blacks” and “Population with ages 5-17”. We also recover an interaction effect between “Non-Hispanic blacks” and “No high school graduation”, which seems to be reflective of this cluster. Consider also the Advantaged Homeowners cluster characterized by stable homeowners who are predominantly white and live in single-unit spousal-households. Our model automatically selects a closely related interaction effect between “Non-Hispanic whites” and “Single units”. Another example is the Single Unattached Mobiles cluster, which is characterized by young, highly educated population living in multi-units structures with high mobility (Bates and Mulry, 2011); the tracts are almost exclusively urban and have an above-average Asian population relative to the national average. Our model selects multiple interaction effects within this group of variables, for example: i) “Moved in 2010 or later” and “Multi-unit structures”; ii) “College or higher degree holders” and “Single person households”; iii) “People speaking Asian languages” and “Multi-unit structures”; iv) “People speaking Asian languages” and “Urban clusters”.

Some of the covariates in Figure 7[right] can also be interpreted in terms of the mindset solutions in Kulzick et al. (2019). In a mindset solution, survey respondents are categorized using factor analysis into six mindsets based on their predicted self-response patterns and demographic characteristics. These mindsets are determined by the demographic characteristics such as age, race, income, home-ownership, presence of children in the household, marital status, internet use, English proficiency, and country of birth. The six mindsets are: Eager Engagers, Fence Sitters, Individuals with a Confidentiality, Head Noddors, Wary Skeptics and Disconnected Doubters. The covariates can be also interpreted in terms of eight segmented tracts: Responsive Suburbia, Main Street Middle, Country Roads, Downtown Dynamic, Student and Military Communities, Sparse Spaces, Multicultural Mosaic, and Rural Delta and Urban Enclaves – see Kulzick et al. (2019) for additional details.

5.4. Conclusions. We propose a framework to obtain models with good predictive accuracy while simultaneously delivering parsimonious and interpretable statistical models. We hope that our framework will help practitioners identify some key factors that influence survey response rates. Insights gathered from our models may be used for targeted follow-up surveys and allocation of resources for advertisements. We hope that our models will help inform the goal of achieving improved census coverage in a timely fashion, while optimizing the operational risks and costs. Our framework can complement and potentially offer an alternative to the LRS metric that is currently used in the US Census Bureau ROAM application.

Acknowledgements. The authors would like to thank Nancy Bates, Tommy Wright and Joanna Fane Lineback from the U.S. Census Bureau for helpful discussions. Thanks also to other researchers from the Centers for Statistical Research and Methodology and Behavioral Science Methods (U.S Census Bureau) for helpful feedback in earlier versions of this work. Any opinions and conclusions expressed herein are those of the authors and do not necessarily represent the views of the U.S. Census Bureau. This research was supported in part, by grants from the Office of Naval Research: ONR-N000141812298 (YIP) and the National Science Foundation: NSF-IIS-1718258 awarded to Rahul Mazumder.

REFERENCES

AGMON, S. (1965). *Lectures on Elliptic Boundary Value Problems*. Van Nostrand, Princeton, NJ.

- BACH, F., JENATTON, R., MAIRAL, J. and OBOZINSKI, G. (2012). Structured Sparsity through Convex Optimization. *Statistical Science* **27** 450–468.
- BATES, N. and MULRY, M. H. (2011). Using a Geographic Segmentation to Understand, Predict, and Plan for Census and Survey Mail Nonresponse. *Journal of Official Statistics* **27** 601–618.
- BERGSTRÄ, J., KOMER, B., ELIASMITH, C. et al. (2015). Hyperopt: a Python library for model selection and hyperparameter optimization. *Computational Science & Discovery* **8** 014008.
- BERTSIMAS, D., KING, A. and MAZUMDER, R. (2016). Best subset selection via a modern optimization lens. *Annals of Statistics* **44**(2) 813–852.
- BIEN, J., TAYLOR, J. and TIBSHIRANI, R. (2013). A lasso for hierarchical interactions. *The Annals of Statistics* **41** 1111–1141.
- BIRMAN, M. S. and SOLOMJAK, M. Z. (1967). Piecewise-polynomial approximations of functions of the classes W_p^α . *Math. USSR-Sbornik* **2**(3) 295–317.
- BRUCE, A., ROBINSON, J. G. and SANDERS, M. V. (2001). Hard-to-count scores and broad demographic groups associated with patterns of response rates in Census 2000. In *Joint Statistical Meeting*.
- BUHLMANN, P. and VAN DE GEER, S. (2011). *Statistics for High-Dimensional Data: Methods, Theory and Applications*, 1st ed. Springer Publishing Company, Incorporated.
- US CENSUS BUREAU (2009). 2010 Census Integrated Communications Campaign Plan: The Success of the Census Is in Our Hands.
- US CENSUS BUREAU (2016). American Community Survey Data Suppression.
- US CENSUS BUREAU (2017). Foundational Communications Models 1.0: the Updated Low Response Score (LRS) and an Internet LRS.
- US CENSUS BUREAU (2019). Planning Database.
- CHEN, T. and GUESTRIN, C. (2016). XGBoost: A Scalable Tree Boosting System. In *Proceedings of the 22nd ACM SIGKDD International Conference on Knowledge Discovery and Data Mining, KDD '16* 785–794. ACM, New York, NY, USA.
- EILERS, P. H. C. and MARX, B. D. (1996). Flexible smoothing with B-splines and penalties. *Statistical Science* **11** 89–121.
- EILERS, P. H. C. and MARX, B. D. (2003). Multivariate calibration with temperature interaction using two-dimensional penalized signal regression. *Chemometrics and Intelligent Laboratory Systems* **66** 159–174.
- ERDMAN, C. and BATES, N. J. (2014). The U.S. Census Bureau Mail Return Rate Challenge: Crowdsourcing to Develop a Hard-to-Count Score.
- ERDMAN, C. and BATES, N. (2016). The Low Response Score (LRS). *Public Opinion Quarterly* **81** 144–156.
- FAN, J. and LI, R. (2001). Variable Selection via Nonconcave Penalized Likelihood and its Oracle Properties. *Journal of the American Statistical Association* **96** 1348–1360.
- FRIEDMAN, J. H. (1991). Multivariate Adaptive Regression Splines. *The Annals of Statistics* **19** 1 – 67.
- FRIEDMAN, J., HASTIE, T. and TIBSHIRANI, R. (2010). Regularization Paths for Generalized Linear Models via Coordinate Descent. *Journal of Statistical Software* **33**.
- HALL, P. and OPSOMER, J. D. (2005). Theory for penalised spline regression. *Biometrika* **92** 105–118.
- HASTIE, T. and TIBSHIRANI, R. (1987). Generalized additive models: some applications. *Journal of the American Statistical Association* **82** 371–386.
- HASTIE, T. J. and TIBSHIRANI, R. J. (1990). *Generalized Additive Models*. Chapman and Hall.
- HASTIE, T., TIBSHIRANI, R. and FRIEDMAN, J. (2001). *The Elements of Statistical Learning. Springer Series in Statistics*. Springer New York Inc., New York, NY, USA.
- HASTIE, T., TIBSHIRANI, R. and WAINWRIGHT, M. (2015). *Statistical Learning with Sparsity: The Lasso and Generalizations*. Chapman & Hall/CRC.
- HAZIMEH, H. and MAZUMDER, R. (2020a). Fast Best Subset Selection: Coordinate Descent and Local Combinatorial Optimization Algorithms. *Oper. Res.* **68** 1517–1537.
- HAZIMEH, H. and MAZUMDER, R. (2020b). Learning Hierarchical Interactions at Scale: A Convex Optimization Approach. In *Proceedings of the Twenty Third International Conference on Artificial Intelligence and Statistics* (S. CHIAPPA and R. CALANDRA, eds.). *Proceedings of Machine Learning Research* **108** 1833–1843. PMLR.
- HAZIMEH, H., MAZUMDER, R. and SAAB, A. (2022). Sparse regression at scale: Branch-and-bound rooted in first-order optimization. *Mathematical Programming* **196** 347–388.
- HAZIMEH, H., MAZUMDER, R. and RADCHENKO, P. (2023). Grouped Variable Selection with Discrete Optimization: Computational and Statistical Perspectives. *The Annals of Statistics* **51** 1–32.
- HUANG, J., HOROWITZ, J. L. and WEI, F. (2010). Variable Selection in Nonparametric Additive Models. *The Annals of Statistics* **38** 2282–2313.
- KAMMANN, E. E. and WAND, M. P. (2003). Geoadditive models. *Journal of the Royal Statistical Society: Series C (Applied Statistics)* **52** 1–18.

- KINGMA, D. P. and BA, J. (2015). Adam: A Method for Stochastic Optimization. In *3rd International Conference on Learning Representations, ICLR 2015, San Diego, CA, USA, May 7-9, 2015, Conference Track Proceedings* (Y. BENGIO and Y. LECUN, eds.).
- KULZICK, R., KAIL, L., MULLENAX, S. et al. (2019). 2020 Census Predictive Models and Audience Segmentation Report.
- LI, K. C., LUE, H. H. and CHEN, C. H. (2000). Interactive tree-structured regression via principal Hessian direction. *Journal of the American Statistical Association* **95** 547–560.
- LI, Y. and RUPPERT, D. (2008). On the Asymptotics of Penalized Splines. *Biometrika* **95** 415–436.
- LIM, M. and HASTIE, T. (2015). Learning Interactions via Hierarchical Group-Lasso Regularization. *Journal of Computational and Graphical Statistics* **24** 627–654.
- LIN, Y. and ZHANG, H. H. (2006). Component selection and smoothing in multivariate nonparametric regression. *The Annals of Statistics* **34** 2272–2297.
- LOU, Y., CARUANA, R., GEHRKE, J. and HOOKER, G. (2013). Accurate Intelligible Models with Pairwise Interactions. In *Proceedings of the 19th ACM SIGKDD International Conference on Knowledge Discovery and Data Mining. KDD '13* 623–631. Association for Computing Machinery, New York, NY, USA.
- LOUNICI, K., PONTIL, M., VAN DE GEER, S. et al. (2011). Oracle Inequalities and Optimal Inference Under Group Sparsity. *The Annals of Statistics* **39** 2164–2204.
- MAMMEN, E., LINTON, O. and NIELSEN, J. (1999). The existence and asymptotic properties of a backfitting projection algorithm under weak conditions. *The Annals of Statistics* **27** 1443–1490.
- MAMMEN, E. and PARK, B. U. (2006). A simple smooth backfitting method for additive models. *The Annals of Statistics* **34** 2252 – 2271.
- MAZUMDER, R. and RADCHENKO, P. (2017). The Discrete Dantzig Selector: Estimating Sparse Linear Models via Mixed Integer Linear Optimization. *IEEE Transactions on Information Theory* **63** (5) 3053 – 3075.
- MAZUMDER, R., RADCHENKO, P. and DEDIEU, A. (2017). Subset selection with shrinkage: Sparse linear modeling when the SNR is low. *arXiv preprint arXiv:1708.03288 (Operations Research, to appear)*.
- MCCULLAGH, P. and NELDER, J. A. (1989). *Generalized linear models* **37**. CRC press.
- MEIER, L., VAN DE GEER, S. and BUHLMANN, P. (2009). High-dimensional additive modeling. *The Annals of Statistics* **37** 3779 – 3821.
- MULE, T. (2012). 2010 Census Coverage Measurement estimation report: Summary of estimates of coverage for persons in the United States DSSD 2010 Census Coverage Measurement Memorandum Series No. 2010-G-01, US Census Bureau.
- NESTEROV, Y. (2003). *Introductory lectures on convex optimization: A basic course* **87**. Springer Science & Business Media.
- NORI, H., JENKINS, S., KOCH, P. and CARUANA, R. (2019). InterpretML: A Unified Framework for Machine Learning Interpretability. *ArXiv abs/1909.09223*.
- ODEN, J. T. and REDDY, J. N. (1976). *An introduction to the mathematical theory of finite elements*. Wiley, New York.
- PEDREGOSA, F., VAROQUAUX, G., GRAMFORT, A. et al. (2011). Scikit-Learn: Machine Learning in Python. *J. Mach. Learn. Res.* **12** 2825–2830.
- RADCHENKO, P. and JAMES, G. M. (2010). Variable Selection Using Adaptive Nonlinear Interaction Structures in High Dimensions. *Journal of the American Statistical Association* **105** 1541–1553.
- RAVIKUMAR, P., LAFFERTY, J., LIU, H. et al. (2009). Sparse additive models. *Journal of the Royal Statistical Society: Series B (Statistical Methodology)* **71** 1009–1030.
- SMITH, T. W. (2014). Hard-to-survey populations in comparative perspective. In *Hard-to-Survey Populations* 21–36. Cambridge University Press, Cambridge.
- STONE, C. J. (1986). The dimensionality reduction principle for generalized additive models. *The Annals of Statistics* 590–606.
- TAN, Z. and ZHANG, C.-H. (2019). Doubly penalized estimation in additive regression with high-dimensional data. *The Annals of Statistics* **47** 2567–2600.
- TOURANGEAU, R., EDWARDS, B., JOHNSON, T. P. et al. (2014). *Hard-to-survey populations*. Cambridge University Press.
- VAN DE GEER, S. (2000). *Empirical Processes in M-Estimation*. Cambridge University Press, Cambridge.
- WAHBA, G. (1990). *Spline Models for Observational Data*. Society for Industrial and Applied Mathematics.
- WOLSEY, L. A. and NEMHAUSER, G. L. (1999). *Integer and combinatorial optimization* **55**. John Wiley & Sons.
- WOOD, S. N. (2006). Low-Rank Scale-Invariant Tensor Product Smooths for Generalized Additive Mixed Models. *Biometrics* **62** 1025–1036.
- WOOD, S. N., LI, Z., SHADDICK, G. et al. (2017). Generalized Additive Models for Gigadata: Modeling the U.K. Black Smoke Network Daily Data. *Journal of the American Statistical Association* **112** 1199–1210.

- WRIGHT, S. J. (2015). Coordinate descent algorithms. *Mathematical Programming* **151** 3–34.
- YAN, X. and BIEN, J. (2017). Hierarchical Sparse Modeling: A Choice of Two Group Lasso Formulations. *Statistical Science* **32** 531–560.
- YANG, Z., ZHANG, A. and SUDJANTO, A. (2021). GAMI-Net: An Explainable Neural Network based on Generalized Additive Models with Structured Interactions. *Pattern Recognit.* **120** 108192.
- YUAN, M. and ZHOU, D.-X. (2016). Minimax optimal rates of estimation in high dimensional additive models. *The Annals of Statistics* **44** 2564–2593.
- ZHANG, C.-H. (2010). Nearly Unbiased Variable Selection Under Minimax Concave Penalty. *The Annals of Statistics* **38** 894–942.
- ZHAO, T. and LIU, H. (2012). Sparse Additive Machine. In *Proceedings of the Fifteenth International Conference on Artificial Intelligence and Statistics* (N. D. LAWRENCE and M. GIROLAMI, eds.). *Proceedings of Machine Learning Research* **22** 1435–1443. PMLR, La Palma, Canary Islands.
- ZSCHECH, P. W., HAMBAUER, S., ZILKER, N., SANDRA; and KRAUS, M. (2022). GAM(e) changer or not? An evaluation of interpretable machine learning models based on additive model constraints. (2022). *ECIS 2022 Research Papers* **106**.

Predicting Census Survey Response Rates with Parsimonious Additive Models and Structured Interactions

APPENDIX: SUPPLEMENTARY MATERIAL

This supplemental document contains some additional results not included in the main body of the paper. In particular, we present

- a detailed discussion of the univariate and bivariate smooth function estimation with splines. These serve as building blocks for modelling main and interaction effects in Section 2.1. The discussion is outlined in Section S1.
- scalability considerations for optimizing ELAAN-I i.e., optimization problem (8) in Section 2.2.
- statistical theory for ELAAN-I: technical details and proofs for Theorem 2.1 in Section 2.3.
- algorithm for optimizing ELAAN-H.
- additional ablation studies.
- Census variable descriptions for Figure 3 in Section 2.2 and Figure 7b in Section 5.3.

This supplement is not entirely self-contained, so readers might need to refer to the main paper.

.....	2
S1 Computational details for optimizing ELAAN-I	2
S1.1 Univariate and bivariate smooth function estimation with splines	2
S1.2 A finite dimensional quadratic program	4
S1.3 Block Coordinate Descent for solving (8)	4
S1.4 Scalability considerations for solving (8)	5
S2 Statistical Theory for ELAAN-I: technical details and proofs	6
S2.1 Notation and assumptions for Theorem 2.1	6
S2.2 Preliminaries and supplementary results	7
S2.3 Proof of Theorem 2.1	7
S2.4 Proof of Corollary 1	8
S2.5 Proof of Lemma S2.1	8
S2.6 Proof of Lemma S2.2	9
S2.7 Proof of Lemma S2.3	10
S3 Algorithms for ELAAN-H with sparse hierarchical interactions: Problem (12)	10
S4 Simulations	11
S4.1 Definition of F1-score	11
S4.2 Ablation Studies	11
S4.3 Tuning Details	13
S5 Data Analysis: Additional Details	13
S5.1 Definition of important Census/American Community Survey variables	13

S1. Computational details for optimizing ELAAN-I.

S1.1. *Univariate and bivariate smooth function estimation with splines.* We discuss how the univariate and bivariate smooth functions are used to model main effects and interaction effects in Section 2.1. The computational details for estimating these building blocks via quadratic optimization are outlined below.

S1.1.1. *One dimensional nonparametric function estimation.* Suppose that we have observations $\{(y_i, u_i)\}_1^n$ corresponding to a univariate response y_i and a univariate predictor $u_i \in [0, 1]$. If the underlying relationship between y and u can be modeled via a twice continuously differentiable (i.e., smooth) function $m(u)$, we can estimate $m(u)$ as a function that minimizes the following objective: $\sum_{i=1}^n (y_i - m(u_i))^2 + \lambda \int (m''(u))^2 du$. This functional optimization problem can be reduced to a finite dimensional quadratic program by using a suitable basis representation for $m(u)$. For example, if all of the u_i 's are distinct and $b_1(u), \dots, b_n(u)$ are the basis functions (for example, cubic splines with knots at the observations u_i , Wahba, 1990; Hastie, Tibshirani and Wainwright, 2015), then we can write $m(u) = \sum_{i=1}^n \gamma_i b_i(u)$. In this case, $\int (m''(u))^2 du = \gamma^\top \mathbf{D} \gamma$, where \mathbf{D} is a positive semidefinite matrix with the (i, l) -th entry given by $\int b_i''(u) b_l''(u) du$.

Instead of using an n -dimensional basis representation for $m(u)$, which is computationally expensive and perhaps statistically redundant, one can choose a smaller number of basis functions, such as $K = O(n^{1/5})$; this leads to a low-rank representation of \mathbf{D} (Hall and Opsomer, 2005; Li and Ruppert, 2008) and hence an improved computational performance. Reducing the number of basis elements from n to K leads to fewer parameters at the expense of a marginal increase in bias (Wahba, 1990), which is often negligible in practice.

The evaluations of the function $m(u)$ at the n data points can be stacked together in the form of a vector $\mathbf{B}\beta$, where \mathbf{B} is an $n \times K$ matrix of basis functions evaluated at the observations, and $\beta \in \mathbb{R}^K$ contains the corresponding basis coefficients that need to be estimated from the data. The univariate function fitting problem then reduces to a regularized least squares problem given by $\min_{\beta \in \mathbb{R}^K} \{\|\mathbf{y} - \mathbf{B}\beta\|_2^2 + \lambda \beta^\top \mathbf{A} \beta\}$.

While many choices of spline bases are available (Wood, 2006; Hastie, Tibshirani and Friedman, 2001), we use penalized B-splines for their appealing statistical and computational properties. Following Eilers and Marx (1996), a second-order finite difference penalty on the coefficients of adjacent B-splines serves as a good discrete approximation to the integral of the squared second-order derivative penalty Ω discussed above. The regularized least squares problem takes the form

$$(S1) \quad \min_{\beta} \|\mathbf{y} - \mathbf{B}\beta\|_2^2 + \lambda \sum_{l=1}^{K-2} (\Delta^2 \beta_l)^2,$$

where K is the number of the B-spline basis functions and $\Delta^2 \beta_l = \beta_l - 2\beta_{l+1} + \beta_{l+2}$ is the second-order finite difference of the coefficients of adjacent B-splines with equidistant knots. We note that the regularization term can be represented in matrix form as $\lambda \|\mathbf{D}\beta\|_2^2$, where $\mathbf{D} \in \mathbb{R}^{(K-2) \times K}$ is a banded matrix with nonzero entries given by $d_{l,l} = 1$, $d_{l,l+1} = -2$ and $d_{l,l+2} = 1$ for $l \in [K-2]$.

S1.1.2. Two dimensional nonparametric function estimation. To model the response as a function of two covariates one can again use reduced rank parameterizations, in the form of multivariate splines (Wahba, 1990), thin-plate splines (Kammann and Wand, 2003), or tensor products of B-splines (Eilers and Marx, 2003; Wood, 2006), for example. We use tensor products of B-splines to model the two-dimensional smooth functions of the form $m(u, v)$, with $(u, v) \in [0, 1]^2$ for concreteness. We start from a low-rank B-spline basis representation for the marginal smooth functions as $m_1(u) = \sum_{k=1}^K \beta_k b_k(u)$ and $m_2(v) = \sum_{l=1}^L \delta_l c_l(v)$, where $\{b_k\}$ and $\{c_l\}$ are B-spline basis functions, and $\{\beta_k\}$, $\{\delta_l\}$ are unknown basis coefficients. We convert the marginal smooth function m_1 into a smooth function of covariates u and v by allowing the coefficients β_k to vary in a smooth fashion with respect to v . Given that we have an available basis for representing smooth functions of v , we can write $\beta_k(v) = \sum_{l=1}^L \delta_{k,l} c_l(v)$ and then arrive at the tensor smooth given by $m(u, v) = \sum_{k=1}^K \sum_{l=1}^L \delta_{k,l} b_k(u) c_l(v)$. We note that the evaluations of the function $m(u, v)$ at the n data points can be stacked together in a vector written as $\mathbf{R}\gamma$. We denote the vectors evaluating the two marginal functional bases, $\{b_k(\cdot)\}$ and $\{c_l(\cdot)\}$, at the i -th data point as $\mathbf{B}_i \in \mathbb{R}^K$ and $\mathbf{C}_i \in \mathbb{R}^L$, respectively. In matrix notation, the model matrix $\mathbf{R} \in \mathbb{R}^{n \times KL}$ can be expressed as $\mathbf{R} = (\mathbf{B} \otimes \mathbf{1}_L) \odot (\mathbf{1}_K \otimes \mathbf{C})$, where operations \otimes and \odot denote Kronecker product and element-wise multiplication respectively. The basis coefficients $\delta_{k,l}$ are appropriately ordered into the vector $\gamma \in \mathbb{R}^{KL}$ via the vectorization operation $\gamma = \text{vec}(\delta) = [\delta_{1,1}, \dots, \delta_{K,1}, \delta_{1,2}, \dots, \delta_{K,2}, \dots, \delta_{1,L}, \dots, \delta_{K,L}]^\top$, where $\delta = [\delta_{k,l}]_{k \in [K], l \in [L]}$ stores the basis coefficients in matrix form.

The smooth 2D estimate can be obtained by making use of tensor products and a discretized version of the smoothness penalty (Eilers and Marx, 2003), given by:

$$(S2) \quad \min_{\gamma} \|\mathbf{y} - \mathbf{R}\gamma\|_2^2 + \lambda_b \sum_{k=1}^K \sum_{l=1}^{L-2} (\Delta_{(1)}^2 \delta_{k,l})^2 + \lambda_c \sum_{l=1}^L \sum_{k=1}^{K-2} (\Delta_{(2)}^2 \delta_{k,l})^2,$$

where $\Delta_{(1)}^2 \delta_{k,l} = \delta_{k,l} - 2\delta_{k,l+1} + \delta_{k,l+2}$ and $\Delta_{(2)}^2 \delta_{k,l} = \delta_{k,l} - 2\delta_{k+1,l} + \delta_{k+2,l}$. The regularization terms above can be compactly represented as quadratic forms in γ as follows:

$$(S3) \quad \min_{\gamma} \|\mathbf{y} - \mathbf{R}\gamma\|_2^2 + \lambda_b \gamma^\top \mathbf{P}_b \gamma + \lambda_c \gamma^\top \mathbf{P}_c \gamma,$$

where $\mathbf{P}_b = (\mathbf{D}^\top \mathbf{D}) \otimes \mathbf{I}_L$ and $\mathbf{P}_c = \mathbf{I}_K \otimes (\mathbf{D}^\top \mathbf{D})$. The regularizer ensures that the coefficients in the same row (or column) of δ vary regularly, leading to a smooth 2D surface.

S1.2. A finite dimensional quadratic program. Problem (2) can be written as a finite-dimensional quadratic program. Using splines to model each of the main-effects and the interaction-effects, one can write the main-effects and interaction-effects as a linear combination of suitable bases elements. More specifically, $\mathbf{f}_j = \mathbf{B}_j \boldsymbol{\beta}_j$, where $\mathbf{B}_j \in \mathbb{R}^{n \times K_j}$ is the model matrix and $\boldsymbol{\beta}_j \in \mathbb{R}^{K_j}$ is the vector of coefficients for each main effect component. Similarly, $\mathbf{f}_{j,k} = \mathbf{B}_{j,k} \boldsymbol{\theta}_{j,k}$, where $\mathbf{B}_{j,k} \in \mathbb{R}^{n \times K_{j,k}}$ is the model matrix and $\boldsymbol{\theta}_{j,k} \in \mathbb{R}^{K_{j,k}}$ is the vector of coefficients for each interaction effect component. Here, K_j and $K_{j,k}$ denote the corresponding dimensions of the bases – in our implementation, all the values K_j are taken to be the same and all the $K_{j,k}$ are taken to be the same as well. We use a penalty function to control the smoothness (i.e., integral of the squared second derivative) of the 1D and 2D components. Writing $\boldsymbol{\beta}$ for the vector obtained by stacking together the coefficients $\boldsymbol{\beta}_j$, $j \in [p]$ for the main-effects, and defining the vector $\boldsymbol{\theta}$ for the interaction effects analogously, we express the optimization problem (2) as follows:

$$\min_{\boldsymbol{\beta}, \boldsymbol{\theta}} \frac{1}{n} \left\| \mathbf{y} - \left[\sum_{j \in [p]} \mathbf{B}_j \boldsymbol{\beta}_j + \sum_{j < k} \mathbf{B}_{j,k} \boldsymbol{\theta}_{j,k} \right] \right\|_2^2 + \lambda_1 \left[\sum_{j \in [p]} \boldsymbol{\beta}_j^T \mathbf{S}_j \boldsymbol{\beta}_j + \sum_{j < k} \boldsymbol{\theta}_{j,k}^T \mathbf{S}_{j,k} \boldsymbol{\theta}_{j,k} \right].$$

Here, $\mathbf{S}_j = \mathbf{D}_j^T \mathbf{D}_j$ and $\mathbf{S}_{j,k} = (\mathbf{D}_j^T \mathbf{D}_j) \otimes \mathbf{I}_k + \mathbf{I}_j \otimes (\mathbf{D}_k^T \mathbf{D}_k)$ are the smoothness penalty matrices for the main effects and the interaction components, respectively. For convenience, we use the same smoothness penalty λ_1 for both the main and the interaction effects, though in general they may be taken to be different.

S1.3. Block Coordinate Descent for solving (8). In our block CD method, the blocks correspond to the basis coefficients for either the main effects $\{\boldsymbol{\beta}_j\}$ or the interaction effects $\{\boldsymbol{\theta}_{j,k}\}$. Given an initialization $(\boldsymbol{\beta}_1^{(0)}, \dots, \boldsymbol{\beta}_p^{(0)}, \boldsymbol{\theta}_{1,2}^{(0)}, \dots, \boldsymbol{\theta}_{p-1,p}^{(0)})$, at every cycle, we sequentially sweep across the main effects and the interaction effects. If we denote the solution after t cycles by $(\boldsymbol{\beta}_1^{(t)}, \dots, \boldsymbol{\beta}_p^{(t)}, \boldsymbol{\theta}_{1,2}^{(t)}, \dots, \boldsymbol{\theta}_{p-1,p}^{(t)})$, then the block of coefficients for j -th main effect $\boldsymbol{\beta}_j^{(t+1)}$ at the cycle $t+1$ is obtained by optimizing (8) with respect to $\boldsymbol{\beta}_j$, with other variables held fixed:

$$(S4) \quad \boldsymbol{\beta}_j^{(t+1)} \in \underset{\boldsymbol{\beta}_j \in \mathbb{R}^{K_j}}{\operatorname{argmin}} G(\boldsymbol{\beta}_1^{(t+1)}, \dots, \boldsymbol{\beta}_{j-1}^{(t+1)}, \boldsymbol{\beta}_j, \boldsymbol{\beta}_{j+1}^{(t)}, \dots, \boldsymbol{\beta}_p^{(t)}, \boldsymbol{\theta}_{1,2}^{(t)}, \dots, \boldsymbol{\theta}_{p-1,p}^{(t)}).$$

Similarly, $\boldsymbol{\theta}_{j,k}^{(t+1)}$, the coefficients for the (j,k) -th interaction effect at cycle $t+1$ are updated as

$$(S5) \quad \boldsymbol{\theta}_{j,k}^{(t+1)} \in \underset{\boldsymbol{\theta}_{j,k} \in \mathbb{R}^{K_{j,k}}}{\operatorname{argmin}} G(\boldsymbol{\beta}_1^{(t+1)}, \dots, \boldsymbol{\beta}_p^{(t+1)}, \boldsymbol{\theta}_{1,2}^{(t+1)}, \dots, \boldsymbol{\theta}_{(j,k)-1}^{(t+1)}, \boldsymbol{\theta}_{j,k}, \boldsymbol{\theta}_{(j,k)+1}^{(t)}, \dots, \boldsymbol{\theta}_{p-1,p}^{(t)}).$$

The block minimization problem (S4) reduces to:

$$(S6) \quad \boldsymbol{\beta}_j^{(t+1)} = \underset{\boldsymbol{\beta}_j \in \mathbb{R}^{K_j}}{\operatorname{argmin}} \psi_j(\mathbf{r}^{(t)}; \boldsymbol{\beta}_j) := \frac{1}{n} \left\| \mathbf{r}^{(t)} - \mathbf{B}_j \boldsymbol{\beta}_j \right\|_2^2 + \lambda_1 \boldsymbol{\beta}_j^T \mathbf{S}_j \boldsymbol{\beta}_j + \lambda_2 \mathbb{1}[\boldsymbol{\beta}_j \neq \mathbf{0}],$$

where $\mathbf{r}^{(t)} = \mathbf{y} - (\sum_{j'=1}^{j-1} \mathbf{B}_{j'} \boldsymbol{\beta}_{j'}^{(t+1)} + \sum_{j'=j+1}^p \mathbf{B}_{j'} \boldsymbol{\beta}_{j'}^{(t)} + \sum_{j' < k'} \mathbf{B}_{j',k'} \boldsymbol{\theta}_{j',k'}^{(t)})$ denotes the residual. A solution to (S6) can be computed in closed form via the following thresholding operator:

$$(S7) \quad \boldsymbol{\beta}_j^{(t+1)} = \begin{cases} \mathbf{0} & \text{if } \psi_j(\mathbf{r}^{(t)}; \mathbf{0}) \leq \min_{\boldsymbol{\beta}_j \neq \mathbf{0}} \psi_j(\mathbf{r}^{(t)}; \boldsymbol{\beta}_j) \\ (\mathbf{B}_j^T \mathbf{B}_j + n\lambda_1 \mathbf{S}_j)^{-1} \mathbf{B}_j^T \mathbf{r}^{(t)} & \text{otherwise.} \end{cases}$$

Similarly, the sub-problem for the interaction effects is

(S8)

$$\theta_{j,k}^{(t+1)} = \underset{\theta_{j,k} \in \mathbb{R}^{K_{j,k}}}{\operatorname{argmin}} \psi_{j,k}(\mathbf{r}^{(t)}; \theta_{j,k}) := \frac{1}{n} \|\mathbf{r}^{(t)} - \mathbf{B}_{j,k} \theta_{j,k}\|_2^2 + \lambda_1 \theta_{j,k}^T \mathbf{S}_{j,k} \theta_{j,k} + \alpha \lambda_2 \mathbb{1}[\theta_{j,k} \neq \mathbf{0}],$$

where $\mathbf{r}^{(t)} = \mathbf{y} - (\sum_{j'=1}^p \mathbf{B}_{j'} \beta_{j'}^{(t+1)} + \sum_{(j',k')=1,2}^{(j,k)-1} \mathbf{B}_{j',k'} \theta_{j',k'}^{(t+1)} + \sum_{(j',k')=(j,k)+1}^{p-1,p} \mathbf{B}_{j',k'} \theta_{j',k'}^{(t)})$. A solution to this problem is given by

(S9)

$$\theta_{j,k}^{(t+1)} = \begin{cases} \mathbf{0} & \text{if } \psi_{j,k}(\mathbf{r}^{(t)}; \mathbf{0}) \leq \min_{\theta_{j,k} \neq \mathbf{0}} \psi_{j,k}(\mathbf{r}^{(t)}; \theta_{j,k}) \\ (\mathbf{B}_{j,k}^T \mathbf{B}_{j,k} + n \lambda_1 \mathbf{S}_{j,k})^{-1} \mathbf{B}_{j,k}^T \mathbf{r}^{(t)} & \text{otherwise.} \end{cases}$$

These block CD updates need to be paired with several computational devices in the form of active set updates, cached matrix factorizations, and warm-starts, among others. We draw inspiration from similar strategies used in CD-based procedures for sparse linear regression (Hazimeh and Mazumder, 2020a; Friedman, Hastie and Tibshirani, 2010), and adapt them to our problem. These devices are discussed in detail in the Supplement Section S1.4.

S1.4. Scalability considerations for solving (8). We draw inspiration from strategies used in CD-based procedures for sparse linear regression (Hazimeh and Mazumder, 2020a; Friedman, Hastie and Tibshirani, 2010), and adapt them to scale cyclic block coordinate descent in Section 2.4 to large problem instances of (8). These include active set updates, cached matrix factorizations and warm-starts. They are explained in more detail below:

S1.4.1. Active set updates. A main computational bottleneck in the block CD approach is the number of passes across the $O(p^2)$ blocks. However, as we anticipate a solution that is sparse (with few nonzero main and interaction effects), we use an active set strategy. We restrict our block CD procedure to a small subset \mathcal{Q} of the $O(p^2)$ variables, with all blocks outside the active set being set to zero. Once the CD algorithm converges on the active set, we check if all blocks outside the active set satisfy the coordinate-wise optimality conditions¹. If there are any violations, we select the corresponding blocks, append them to the current active set, and then rerun our block CD procedure. As there are finitely many active sets, the algorithm is guaranteed to converge – in practice, with warm-start continuation (discussed below), the number of active set updates is quite small, and the algorithm is found to converge quite quickly.

S1.4.2. Cached matrix factorizations. The updates (S7) and (S9) require computing a matrix inverse. In particular, if a block is nonzero, we need to compute a linear system solution of the form: $\mathbf{A}_l^{-1} \mathbf{b}_l$ where $\mathbf{A}_l = \mathbf{B}_l^T \mathbf{B}_l + n \lambda_1 \mathbf{S}_l$. We note that matrix \mathbf{A}_l is fixed throughout the CD updates and is independent of the choice of the sparsity regularization parameter λ_2 – hence, we pre-compute a matrix factorization for \mathbf{A}_l (for example, an *LU* decomposition) and use it to compute the solution to the linear system. As the dimension of \mathbf{A}_l equals the number of basis coefficients, which is small, this can be done quite efficiently.

S1.4.3. Warm-starts. We use our CD procedure to compute a path of solutions to (8) for a 2D grid of tuning parameters $(\lambda_1, \lambda_2) \in \{\lambda_1^{(l)}\}_{l=0}^L \times \{\lambda_2^{(m)}\}_{m=0}^M$, where λ_1 corresponds to the smoothness parameter and λ_2 the sparsity parameter. Here, $\lambda_1^{(l)} > \lambda_1^{(l+1)}$ for all l ,

¹That is, we check if optimal solutions to (9) and (10) are zero for all blocks outside \mathcal{Q} .

and $\lambda_2^{(m)} > \lambda_2^{(m+1)}$ for all m . When $\lambda_1 = \lambda_1^{(0)}$ (most regularized), we compute a sequence of solutions across the λ_2 -values (from large to small values): a solution obtained at $(\lambda_1^{(0)}, \lambda_2^{(m)})$ is used to initialize our CD procedure for the value $(\lambda_1^{(0)}, \lambda_2^{(m+1)})$. As the number of nonzeros in a solution to (8) generally increases with λ_2 -values, our CD procedure for $(\lambda_1^{(0)}, \lambda_2^{(m+1)})$ uses an active set that is slightly larger than the active set² corresponding to the solution at $(\lambda_1^{(0)}, \lambda_2^{(m)})$. Once we have traced a full path over λ_2 , we use warm-starts in the lateral direction across the space of λ_1 . For all $l \geq 0$, to obtain a solution to (8) at $(\lambda_1^{(l+1)}, \lambda_2^{(m)})$, we use the solution at $(\lambda_1^{(l)}, \lambda_2^{(m)})$ as a warm-start.

S2. Statistical Theory for ELAAN-I: technical details and proofs.

S2.1. Notation and assumptions for Theorem 2.1. Given a candidate regression function $f : [0, 1]^p \mapsto \mathbb{R}$ of the form $f(\mathbf{x}) = \sum_{j \in [p]} f_j(x_j) + \sum_{j < k} f_{j,k}(x_j, x_k)$, we define its sparsity level as

$$G(f) = \sum_{j \in [p]} \mathbb{1}[\mathbf{f}_j \neq \mathbf{0}] + \sum_{j < k} \mathbb{1}[\mathbf{f}_{j,k} \neq \mathbf{0}].$$

To ensure identifiability of the additive representation for $f(\mathbf{x})$ additional restrictions need to be imposed on the components f_j and $f_{j,k}$. For the simplicity of the presentation, we avoid specifying a particular set of restrictions and treat every representation of f as equivalent, with the understanding that one particular representation is used when evaluating quantities such as $G(f)$.

We write $\|\cdot\|_{L_2}$ for the L_2 norm of a real-valued function on $[0, 1]^2$ or $[0, 1]$. We focus on the case where \mathcal{C}_1 and \mathcal{C}_2 are L_2 -Sobolev spaces. More specifically, we let

$$\mathcal{C}_2 = \left\{ g(u, v) : [0, 1]^2 \mapsto \mathbb{R}, \|g\|_{L_2} + \left\| \frac{\partial^2 g}{\partial u^2} \right\|_{L_2} + \left\| \frac{\partial^2 g}{\partial u \partial v} \right\|_{L_2} + \left\| \frac{\partial^2 g}{\partial v^2} \right\|_{L_2} < \infty \right\}$$

$$\Omega(g) = \left\| \frac{\partial^2 g}{\partial u^2} \right\|_{L_2}^2 + \left\| \frac{\partial^2 g}{\partial u \partial v} \right\|_{L_2}^2 + \left\| \frac{\partial^2 g}{\partial v^2} \right\|_{L_2}^2,$$

and also let $\mathcal{C}_1 = \{h : [0, 1] \mapsto \mathbb{R}, \|h\|_{L_2} + \|h''\|_{L_2} < \infty\}$, $\Omega(h) = \|h''\|_{L_2}^2$. We define the corresponding space of additive functions with interactions as

$$\mathcal{C}_{\text{gr}} = \{f : [0, 1]^p \mapsto \mathbb{R}, f(\mathbf{x}) = \sum_{j \in [p]} f_j(x_j) + \sum_{j < k} f_{j,k}(x_j, x_k), f_j \in \mathcal{C}_1, f_{j,k} \in \mathcal{C}_2, G(f) \leq K\},$$

where K is some arbitrarily large universal constant, and let

$$\Omega_{\text{gr}}(f) = \sum_{j \in [p]} \Omega(f_j) + \sum_{j < k} \Omega(f_{j,k}).$$

We associate each $f \in \mathcal{C}_{\text{gr}}$ with the vector $\mathbf{f} = \sum_{j \in [p]} \mathbf{f}_j + \sum_{j < k} \mathbf{f}_{j,k}$, where $\mathbf{f}_j = (f_j(x_{1j}), \dots, f_j(x_{nj}))$ and $\mathbf{f}_{j,k} = (f_{j,k}(x_{1j}, x_{1k}), \dots, f_{j,k}(x_{nj}, x_{nk}))$.

We assume that the observed data follows the model $\mathbf{y} = \mathbf{f}^* + \boldsymbol{\epsilon}$, where $\mathbf{f}^* = (f(\mathbf{x}_1), \dots, f(\mathbf{x}_n))$ is the vector representation of a function $f^* : [0, 1]^p \mapsto \mathbb{R}$, and the elements of $\boldsymbol{\epsilon}$ are independent $N(0, \sigma^2)$ with $\sigma > 0$.

²This is usually taken to be 1-10% larger than the current active set, and is chosen in a greedy fashion from among the main and interaction effects lying outside the current active set.

S2.2. Preliminaries and supplementary results. We will prove a more general result by replacing the 2-nd derivative in the definition of \mathcal{C}_{gr} and Ω_{gr} with an m -th derivative, and redefining r_n as $n^{-m/(2m+2)}$. Theorem 2.1 will then follow as a special case corresponding to $m = 2$. The more general prediction error bound extends the result in Theorem 2 of Lin and Zhang (2006), which is established for the fixed p setting, from the main effects models to the interaction models. When $\log(p) \lesssim n^{1/(m+1)}$, the prediction error rate matches the optimal bivariate rate of $n^{-m/(m+1)}$.

We extend the domain of $\|\cdot\|_n$ from vectors in \mathbb{R}^n to real-valued functions on $[0, 1]^p$ by letting $\|\cdot\|_n$ be the empirical L_2 -norm. Thus, given a function h , we let $\|h\|_n = [\sum_{i=1}^n h(\mathbf{x}_i)^2/n]^{1/2}$. This extension is consistent in the sense that $\|f\|_n = \|\mathbf{f}\|_n$ for $f \in \mathcal{C}_{\text{gr}}$. By analogy with the $\|\cdot\|_n$ notation, we define $(\epsilon, \mathbf{v})_n = (1/n) \sum_{i=1}^n \epsilon_i v_i$ for each $\mathbf{v} \in \mathbb{R}^n$. For the simplicity of the presentation, we use the double-index notation f_{jj} for the main effect components f_j of functions $f \in \mathcal{C}_{\text{gr}}$ and then take advantage of the additive representation

$$\sum_{j \in [p]} f_j(x_j) + \sum_{j < k} f_{j,k}(x_j, x_k) = \sum_{j \leq k} f_{j,k}(x_j, x_k).$$

We also define $\tilde{\Omega}(f_{j,k}) = \sqrt{\Omega(f_{j,k})}$ and $\tilde{\Omega}_{\text{gr}}(f) = \sum_{j \leq k} \sqrt{\Omega(f_{j,k})}$.

We let $\mathcal{J} = \{(j, k) \in [p] \times [p], \text{ s.t. } j \leq k\}$. Given $J \subseteq \mathcal{J}$, we define functional classes $\mathcal{F}(J) = \{f : f(\mathbf{x}) = \sum_{(j,k) \in J} f_{j,k}(x_j, x_k), f_{j,k} \in \mathcal{C}_2\}$ and $\mathcal{H}(J) = \{h : h \in \mathcal{F}(J), \|h\|_n/(r_n + \tilde{\Omega}_{\text{gr}}(h)) \leq 1\}$; we also let $\mathcal{F}_s = \{f : f \in \mathcal{C}_{\text{gr}}, G(f) \leq s\}$ for every natural s . Given a positive constant δ and a metric space \mathcal{H} endowed with the norm $\|\cdot\|$, we use the standard notation and write $H(\delta, \mathcal{H}, \|\cdot\|)$ for the δ -entropy of \mathcal{H} with respect to $\|\cdot\|$. More specifically, $H(\delta, \mathcal{H}, \|\cdot\|)$ is the natural logarithm of the smallest number of balls with radius δ needed to cover \mathcal{H} . The following result, proved in Section S2.5, bounds the entropy of $\mathcal{H}(J)$.

LEMMA S2.1. $H(u, \mathcal{H}(J), \|\cdot\|_n) \lesssim (1/u)^{2/m}$ for $u \in (0, 1)$.

Let $M = K(K+1)/2$. We will need the following maximal inequalities, which are proved in Sections S2.6 and S2.7, respectively.

LEMMA S2.2. Suppose that $J \subseteq \mathcal{J}$ and $|J| \leq M$. Then, with probability at least $1 - e^{-t}$, inequality

$$(\epsilon/\sigma, \mathbf{f})_n \lesssim \left[r_n + \sqrt{t/n} \right] \|\mathbf{f}\|_n + \left[r_n^2 + r_n \sqrt{t/n} \right] \tilde{\Omega}_{\text{gr}}(f)$$

holds uniformly over $f \in \mathcal{F}(J)$.

LEMMA S2.3. With probability at least $1 - \epsilon$, inequality

$$\begin{aligned} (\epsilon/\sigma, \mathbf{f})_n &\lesssim \left[r_n + \sqrt{\frac{\log(ep)}{n}} + \sqrt{\frac{\log(1/\epsilon)}{n}} \right] \|\mathbf{f}\|_n \\ &\quad + \left[r_n^2 + r_n \sqrt{\frac{\log(ep)}{n}} + r_n \sqrt{\frac{\log(1/\epsilon)}{n}} \right] \tilde{\Omega}_{\text{gr}}(f) \end{aligned}$$

holds uniformly over $f \in \mathcal{F}_M$.

S2.3. Proof of Theorem 2.1. Consider an arbitrary function $f \in \mathcal{C}_{\text{gr}}$. For the remainder of the proof, all universal constants will be chosen independently of f . Because f is feasible for optimization problem (5), we have the following inequality:

(S10)

$$\|\hat{\mathbf{f}}_n - \mathbf{f}^*\|_n^2 + \lambda_n \Omega_{\text{gr}}(\hat{f}_n) + \mu_n G(\hat{f}_n) \leq \|\mathbf{f} - \mathbf{f}^*\|_n^2 + 2(\epsilon, \hat{\mathbf{f}}_n - \mathbf{f})_n + \lambda_n \Omega_{\text{gr}}(f) + \mu_n G(f).$$

Applying Lemma S2.3 with $f = \hat{f}_n - f$ and $\epsilon = (ep)^{-1}$, we derive that, with probability at least $1 - 1/p$,

$$(S11) \quad \begin{aligned} (\epsilon/\sigma, \hat{\mathbf{f}}_n - \mathbf{f})_n &\leq c_1 \left[r_n + \sqrt{\frac{\log(ep)}{n}} \right] \|\hat{\mathbf{f}}_n - \mathbf{f}\|_n \\ &\quad + a_2 \left[r_n^2 + r_n \sqrt{\frac{\log(ep)}{n}} \right] \tilde{\Omega}_{\text{gr}}(\hat{f}_n - f) \end{aligned}$$

for some universal constants a_1 and a_2 . For the remainder of the proof we restrict our attention to the random event on which (S11) holds. Multiplying inequality (S10) by two, using (S11), and letting

$$\tau_n := 2c_1\sigma \left[r_n + \sqrt{\frac{\log(ep)}{n}} \right], \quad \tilde{\lambda}_n := 4a_2\sigma \left[r_n^2 + r_n \sqrt{\frac{\log(ep)}{n}} \right], \quad \text{and } \lambda_n \geq \tilde{\lambda}_n,$$

we derive

$$2\|\hat{\mathbf{f}}_n - \mathbf{f}^*\|_n^2 + 2\lambda_n \Omega_{\text{gr}}(\hat{f}_n) + 2\mu_n G(\hat{f}_n) \leq 2\|\mathbf{f} - \mathbf{f}^*\|_n^2 + 2\tau_n \|\hat{\mathbf{f}}_n - \mathbf{f}\|_n + \tilde{\lambda}_n \tilde{\Omega}_{\text{gr}}(\hat{f}_n - f) + 2\lambda_n \Omega_{\text{gr}}(f) + 2\mu_n G(f).$$

Applying inequalities $2\tau_n \|\hat{\mathbf{f}}_n - \mathbf{f}^*\|_n \leq \tau_n^2 + \|\hat{\mathbf{f}}_n - \mathbf{f}^*\|_n^2$ and $2\tau_n \|\mathbf{f}^* - \mathbf{f}\|_n \leq \tau_n^2 + \|\mathbf{f} - \mathbf{f}^*\|_n^2$, we arrive at

$$\begin{aligned} 2\|\hat{\mathbf{f}}_n - \mathbf{f}^*\|_n^2 + 2\lambda_n \Omega_{\text{gr}}(\hat{f}_n) + 2\mu_n G(\hat{f}_n) &\leq \|\hat{\mathbf{f}}_n - \mathbf{f}^*\|_n^2 + 3\|\mathbf{f} - \mathbf{f}^*\|_n^2 + 2\tau_n^2 \\ &\quad + \tilde{\lambda}_n [\tilde{\Omega}_{\text{gr}}(\hat{f}_n) + \tilde{\Omega}_{\text{gr}}(f)] + 2\lambda_n \Omega_{\text{gr}}(f) + 2\mu_n G(f). \end{aligned}$$

Taking into account inequality $\tilde{\Omega}_{\text{gr}}(\tilde{f}) \lesssim G(\tilde{f}) + \Omega_{\text{gr}}(\tilde{f})$, which holds for any $\tilde{f} \in \mathcal{C}_{\text{gr}}$, we conclude that

$$(S12) \quad \|\hat{\mathbf{f}}_n - \mathbf{f}^*\|_n^2 + \lambda_n \Omega_{\text{gr}}(\hat{f}_n) + 2\mu_n G(\hat{f}_n) \leq 3\|\mathbf{f} - \mathbf{f}^*\|_n^2 + a_3 \tau_n^2 + 2\lambda_n \Omega_{\text{gr}}(f) + 2\mu_n G(f)$$

for some universal constant a_3 . \square

S2.4. Proof of Corollary 1. The stated prediction error bound is a direct consequence of the bound in Theorem 2.1, hence we only need to establish the sparsity bound. Taking $f = f^*$, we rewrite inequality (S12) as follows:

$$(S13) \quad \|\hat{\mathbf{f}}_n - \mathbf{f}^*\|_n^2 + \lambda_n \Omega_{\text{gr}}(\hat{f}_n) + 2\mu_n G(\hat{f}_n) \leq a_3 \tau_n^2 + 2\lambda_n \Omega_{\text{gr}}(f^*) + 2\mu_n G(f^*).$$

Provided that constant c_2 in the lower bound for μ_n is sufficiently large, we then have $G(\hat{f}_n) - G(f^*) < 1$, which implies $G(\hat{f}_n) \leq G(f^*)$.

We now focus on the classical asymptotic setting, where p is fixed and n tends to infinity, under the conditions of Corollary 1. Noting that $1/n = o(r_n^2)$ and repeating the arguments in the proofs of Theorem 2.1 and Corollary 1 with $\epsilon = \exp(-nr_n^2)$, we conclude that inequality (S13) and the accompanying sparsity bound $G(\hat{f}_n) \leq G(f^*)$ hold with probability tending to one. Imposing an additional requirement that $\lambda_n = O(r_n^2 + \log(ep)/n)$ and $\mu_n = O(r_n^2 + \log(ep)/n)$ then leads to $\|\hat{\mathbf{f}}_n - \mathbf{f}^*\|_n^2 = O(r_n^2 + \log(ep)/n)$. \square

S2.5. Proof of Lemma S2.1. We will establish the stated entropy bound for a somewhat larger functional space $\mathcal{H}'_J = \{h : h \in \mathcal{F}(J), \|h\|_n + \tilde{\Omega}_{\text{gr}}(h) \leq 1\}$. We treat m as a fixed universal constant in all inequalities that follow.

Consider an arbitrary $g \in \mathcal{C}_2$. By the Sobolev embedding theorem (for example, Oden and Reddy, 1976, Theorem 3.13), we can write g as a sum of a polynomial of degree $m - 1$ and a function \tilde{g} that satisfies $\|\tilde{g}\|_{L_2} \lesssim \tilde{\Omega}(g)$, where we note that $\tilde{\Omega}(g) = \tilde{\Omega}(\tilde{g})$. Applying Lemma

10.9 in [Van de Geer \(2000\)](#), which builds on the interpolation inequality of [Agmon \(1965\)](#), we derive $\|\tilde{g}\|_\infty \lesssim \tilde{\Omega}(\tilde{g})$. Thus, $\mathcal{H}'_J \subseteq \{p + \tilde{h} : p \in \mathcal{P}_J, \tilde{h} \in \tilde{\mathcal{H}}_J\}$, where

$$\mathcal{P}_J = \{p : p(\mathbf{x}) = \sum_{(j,k) \in J} \sum_{l=0}^{m-1} \sum_{q=0}^{m-1} \alpha_{j,k,l,q} x_j^l x_k^q, \alpha_{j,k,l,q} \in \mathbb{R}, \|p\|_n \leq 2\}$$

$$\tilde{\mathcal{H}}_J = \{\tilde{h} : \tilde{h} \in \mathcal{F}(J), \tilde{\Omega}_{\text{gr}}(\tilde{h}) \leq 1, \|\tilde{h}_{j,k}\|_\infty \lesssim \tilde{\Omega}(\tilde{h}_{j,k}) \forall (j,k) \in J\}.$$

Bound $\|p\|_n \leq 2$ in the definition of \mathcal{P}_J holds because if $h = p + \tilde{h}$ for $h \in \mathcal{H}'_J$ and $\tilde{h} \in \tilde{\mathcal{H}}_J$, then $\|p + \tilde{h}\|_n \leq 1$ and $\|\tilde{h}\|_n \leq \tilde{\Omega}_{\text{gr}}(\tilde{h}) \leq 1$. Consequently,

$$(S14) \quad H(u, \mathcal{H}(J), \|\cdot\|_n) \leq H(u, \mathcal{H}'_J, \|\cdot\|_n) \leq H(u/2, \mathcal{P}_J, \|\cdot\|_n) + H(u/2, \tilde{\mathcal{H}}_J, \|\cdot\|_\infty),$$

where we used the fact that the unit ball with respect to the $\|\cdot\|_\infty$ -norm is contained within the corresponding ball with respect to the $\|\cdot\|_n$ -norm. We note that \mathcal{P}_J is a ball of radius 2, with respect to the $\|\cdot\|_n$ -norm, in a linear functional space of dimension $\lesssim |J| + 1$. Hence, $H(u/2, \mathcal{P}_J, \|\cdot\|_n) \lesssim |J| + |J| \log(1/u)$ by, for example, Corollary 2.6 in [Van de Geer \(2000\)](#). Thus, the result of Lemma [S2.1](#) follows from [S14](#) if we also establish that $H(\delta, \tilde{\mathcal{H}}_J, \|\cdot\|_\infty) \lesssim |J|(1/\delta)^{2/m}$ for $\delta \in (0, 1)$.

We complete the proof by deriving the stated bound on $H(\delta, \tilde{\mathcal{H}}_J, \|\cdot\|_\infty)$. We represent $\tilde{\mathcal{H}}_J$ as

$$\left\{ \tilde{h} : \tilde{h}(\mathbf{x}) = \sum_{(j,k) \in J} \lambda_{(j,k)} g_{(j,k)}(x_{(j,k)}), \sum_{(j,k) \in J} |\lambda_{(j,k)}| \leq 1, g_{(j,k)} \in \mathcal{C}_2, \tilde{\Omega}(g_{(j,k)}) \leq 1, \|g_{(j,k)}\|_\infty \leq 1 \right\}.$$

Given functions $\tilde{h}(\mathbf{x}) = \sum_{(j,k) \in J} \lambda_{(j,k)} g_{(j,k)}(x_j, x_k)$ and $\tilde{h}'(\mathbf{x}) = \sum_{(j,k) \in J} \lambda'_{(j,k)} g'_{(j,k)}(x_j, x_k)$ in $\tilde{\mathcal{H}}_J$, we have

$$\begin{aligned} \|\tilde{h} - \tilde{h}'\|_\infty &\leq \left\| \sum_{(j,k) \in J} \lambda_{(j,k)} g_{(j,k)} - \sum_{(j,k) \in J} \lambda_{(j,k)} g'_{(j,k)} \right\|_\infty + \left\| \sum_{(j,k) \in J} \lambda_{(j,k)} g'_{(j,k)} - \sum_{(j,k) \in J} \lambda'_{(j,k)} g'_{(j,k)} \right\|_\infty \\ &\leq \max_{(j,k) \in J} \|g_{(j,k)} - g'_{(j,k)}\|_\infty \sum_{(j,k) \in J} |\lambda_{(j,k)}| + \max_{(j,k) \in J} \|g'_{(j,k)}\|_\infty \sum_{(j,k) \in J} |\lambda_{(j,k)} - \lambda'_{(j,k)}| \\ &\leq \max_{(j,k) \in J} \|g_{(j,k)} - g'_{(j,k)}\|_\infty + \sum_{(j,k) \in J} |\lambda_{(j,k)} - \lambda'_{(j,k)}|. \end{aligned}$$

Consequently, if we let $\mathcal{G} = \{g : g \in \mathcal{C}_2, \tilde{\Omega}(g) \leq 1, \|g\|_\infty \leq 1\}$, let $\|\cdot\|_1$ denote the ℓ_1 -norm, and let B_1^d denote a unit ℓ_1 -ball in \mathbb{R}^d , then

$$H(\delta, \tilde{\mathcal{H}}_J, \|\cdot\|_\infty) \leq |J| H(\delta/2, \mathcal{G}, \|\cdot\|_\infty) + H(\delta/2, B_1^{|J|}, \|\cdot\|_1).$$

By the results in [Birman and Solomjak \(1967\)](#), $H(\delta/2, \mathcal{G}, \|\cdot\|_\infty) \lesssim (1/\delta)^{2/m}$. By the standard bounds on the covering numbers of a norm ball, $H(\delta/2, B_1^{|J|}, \|\cdot\|_1) \lesssim |J| + |J| \log(1/\delta)$. Consequently, $H(\delta, \tilde{\mathcal{H}}_J, \|\cdot\|_\infty) \lesssim |J|(1/\delta)^{2/m}$ for $\delta \in (0, 1)$. \square

S2.6. Proof of Lemma [S2.2](#). We note that $\|h\|_n \leq r_n$ and $\tilde{\Omega}_{\text{gr}}(h) \leq 1$ for every $h \in \mathcal{H}(J)$. By Lemma 12 in the supplementary material for [Tan and Zhang \(2019\)](#) (cf. Corollary 8.3 in [Van de Geer, 2000](#)),

$$(S15) \quad \sup_{h \in \mathcal{H}(J)} (\epsilon/\sigma, \mathbf{h})_n \lesssim n^{-1/2} \int_0^{r_n} \sqrt{H(u, \mathcal{H}(J), \|\cdot\|_n)} du + r_n \sqrt{t/n}$$

with probability at least $1 - e^{-t}$.

We note that $r_n = n^{-m/(2m+2)}$ and, thus, $n^{-1/2}r_n^{(m-1)/m} = r_n^2$. Using Lemma S2.1 to bound the entropy, we derive

$$n^{-1/2} \int_0^{r_n} \sqrt{H(u, \mathcal{H}(J), \|\cdot\|_n)} du \lesssim n^{-1/2} \int_0^{r_n} u^{-1/m} du \lesssim n^{-1/2} r_n^{(m-1)/m} = r_n^2.$$

Applying bound (S15), we conclude that

$$\sup_{h \in \mathcal{H}(J)} (\epsilon/\sigma, \mathbf{h})_n \lesssim r_n^2 + r_n \sqrt{t/n}$$

with probability at least $1 - e^{-t}$. The statement of the lemma is then a consequence of the fact that for every $f \in \mathcal{F}(J)$, function $f/[\|f\|_n r_n^{-1} + \tilde{\Omega}_{\text{gr}}(f)]$ falls in the class $\mathcal{H}(J)$. \square

S2.7. Proof of Lemma S2.3. Let M_s denote the number of distinct subsets of \mathcal{J} that have size M or smaller. We note that $\log(M_s) \leq 4M \log(ep)$ and, thus, $M_s e^{-t} \leq e^{4M \log(ep) - t}$. Applying Lemma S2.2 together with the union bound, we derive that, with probability at least $1 - e^{4M \log(ep) - t}$, inequality

$$(\epsilon/\sigma, \mathbf{f})_n \lesssim \left[r_n + \sqrt{t/n} \right] \|\mathbf{f}\|_n + \left[r_n^2 + r_n \sqrt{t/n} \right] \tilde{\Omega}_{\text{gr}}(f)$$

holds uniformly over $f \in \mathcal{F}_M$. We complete the proof by noting that for $t = 4M \log(ep) + \log(1/\epsilon)$ the above inequality becomes

$$\begin{aligned} (\epsilon/\sigma, \mathbf{f})_n &\lesssim \left[r_n + \sqrt{\frac{\log(ep)}{n}} + \sqrt{\frac{\log(1/\epsilon)}{n}} \right] \|\mathbf{f}\|_n \\ &\quad + \left[r_n^2 + r_n \sqrt{\frac{\log(ep)}{n}} + r_n \sqrt{\frac{\log(1/\epsilon)}{n}} \right] \tilde{\Omega}_{\text{gr}}(f), \end{aligned}$$

and the corresponding lower-bound on the probability simplifies to $1 - \epsilon$. \square

S3. Algorithms for ELAAN-H with sparse hierarchical interactions: Problem (12).

Similar to the case of (8), and with the computational speed in mind, we present approximate methods to obtain good solutions to (12). As mentioned earlier, these approximate solutions can be used to initialize MIP-based approaches for (12) to improve the solution, and/or to certify the quality of these approximate solutions following Bertsimas, King and Mazumder (2016); Hazimeh and Mazumder (2020a).

Our first step is to reduce the number of main and interaction effects in (12) by making use of the family of solutions available from (8). We consider the union of supports available from the family of solutions obtained from (8), across the 2D grid of tuning parameters λ_1, λ_2 . Let $\mathcal{M} \subset [p]$ and $\mathcal{I} \subset [p(p-1)/2]$ denote the sets of all nonzero main effects and interactions effects, respectively³, encountered along the 2D path of solutions to (8). We form a reduced version of problem (12) with $z_i = 0, i \notin \mathcal{M}$ and $z_{j,k} = 0$ for all $(j,k) \notin \mathcal{I}$. Let us denote the reduced problem by $\mathcal{P}(\mathcal{M}, \mathcal{I})$. We consider a convex relaxation of $\mathcal{P}(\mathcal{M}, \mathcal{I})$, denoted by $\mathcal{P}^R(\mathcal{M}, \mathcal{I})$, where all binary variables $\{z_i\}, \{z_{j,k}\}$ in $\mathcal{P}(\mathcal{M}, \mathcal{I})$ are relaxed to the interval $[0, 1]$. As the sizes of \mathcal{M} and \mathcal{I} are generally small, it is computationally feasible to solve the relaxation $\mathcal{P}^R(\mathcal{M}, \mathcal{I})$ – we let $\{z_i^R\}$ and $\{z_{j,k}^R\}$ denote a solution to this relaxation. Following Hazimeh and Mazumder (2020b), it can be shown that this solution satisfies the strong hierarchy constraint (almost surely). To obtain a feasible solution to Problem (12), we apply a relax-and-round procedure. For the rounding step, we consider a threshold $\tau \in (0, 1)$

³If \mathcal{I} includes an interaction (j, k) where main-effect j is not included in \mathcal{M} , we expand \mathcal{M} to include j . This way, we make sure that all interaction effects have the corresponding main effects included in \mathcal{M} .

and obtain $\tilde{z}_i = \mathbb{1}[z_i^R > \tau]$ for all $i \in \mathcal{M}$ and $\tilde{z}_{j,k} = \mathbb{1}[z_{j,k}^R > \tau]$ for all $(j, k) \in \mathcal{I}$. We set $\tilde{z}_i = 0$, $i \notin \mathcal{M}$; and $\tilde{z}_{j,k} = 0$ for all $(j, k) \notin \mathcal{I}$. It can be verified that this rounding procedure maintains strong hierarchy. Finally, we perform a ‘polishing’ step where we solve (2) restricted to the support defined by $\{\tilde{z}_i\}_i$ and $\{\tilde{z}_{j,k}\}_{j,k}$.

Related Work. In contrast to Problem (8), the regularization penalty in problem (12) is not separable across the blocks due to the overlapping groups created by the strong hierarchy constraint. Hence, the CD-based procedures discussed for (8) do not apply to the hierarchical setting. To the best of our knowledge, there are no prior specialized algorithms for (12) that apply to the scale that we consider here. In fact, even in the linear regression setting, current algorithms for problems with a hierarchy constraint are somewhat limited in terms of the problem-scales they can address. The sole exceptions appear to be the convex optimization based approaches of [Lim and Hastie \(2015\)](#); [Hazimeh and Mazumder \(2020b\)](#), which can address sparse linear regression problems with a large number of features and a small number of observations.

S4. Simulations.

S4.1. *Definition of F1-score.* F1-score is a harmonic mean of precision and recall:

$$(S16) \quad \text{F1-score} = 2 * \frac{\text{Precision} \times \text{Recall}}{\text{Precision} + \text{Recall}},$$

where

$$\text{Precision} = \frac{\# \text{ of True Positives}}{\# \text{ of True Positives} + \# \text{ of False Positives}},$$

$$\text{Recall} = \frac{\# \text{ of True Positives}}{\# \text{ of True Positives} + \# \text{ of False Negatives}}$$

For example, if we have 10 main effects and the true support is given by $\{1, 1, 1, 1, 0, 0, 0, 0, 0, 0\}$ and the recovered support is $\{1, 1, 1, 0, 0, 1, 1, 0, 0, 0\}$, the F1-score is 66.67%.

S4.2. *Ablation Studies.* In this section, we perform ablation studies to investigate (i) the effect of number of basis elements on out-of-sample generalization (ii) the performance of our estimator when the error distribution of ϵ is not normally distributed.

S4.2.1. *Effect of number of basis functions.* We study the effect of number of basis functions on the model performance. We consider 3 different configurations: $\{(K_i = 5, K_{ij} = 3 \times 3), (K_i = 10, K_{ij} = 5 \times 5), (K_i = 20, K_{ij} = 8 \times 8)\}$. The results are reported in Table S1. As expected, we observe that the performance generally degrades when the number

TABLE S1

Average integrated squared error for different configurations of basis elements. “No” in Smoothing column indicates $\lambda_1 = 0$. “Yes” in Smoothing column indicates λ_1 is tuned via cross-validation. Note that for all cases λ_2 is tuned via cross-validation.

Model	α	Smoothing	K_i	N_{train}	100	200	400	1000
				K_{ij}				
ELAAN-I	1.0	Yes	20	8x8	0.269 (0.014)	0.100 (0.004)	0.0444 (0.0016)	0.0161 (0.0005)
		Yes	10	5x5	0.193 (0.012)	0.075 (0.002)	0.0412 (0.0016)	0.0135 (0.0004)
		Yes	5	3x3	0.162 (0.005)	0.088 (0.002)	0.0579 (0.0007)	0.0445 (0.0003)
		No	5	3x3	0.177 (0.005)	0.100 (0.003)	0.0609 (0.0008)	0.0463 (0.0004)
	1.5	Yes	20	8x8	0.270 (0.013)	0.116 (0.006)	0.0405 (0.0013)	0.0157 (0.0004)
		Yes	10	5x5	0.220 (0.013)	0.077 (0.002)	0.0353 (0.0011)	0.0135 (0.0004)
		Yes	5	3x3	0.174 (0.006)	0.087 (0.002)	0.0577 (0.0005)	0.0448 (0.0003)
		No	5	3x3	0.188 (0.007)	0.095 (0.002)	0.0603 (0.0007)	0.0455 (0.0003)

TABLE S2
Integrated squared error for ELAAN-I, EBM and GAMI-Net when the error distribution is skewed or heteroskedastic.

ϵ -distribution	N_{train}	100	200	400
	Model			
Skewed	EBM	0.275 ± 0.004	0.171 ± 0.002	0.103 ± 0.001
	GAMI-Net	0.292 ± 0.007	0.123 ± 0.004	0.060 ± 0.004
	ELAAN-I	0.214 ± 0.008	0.084 ± 0.003	0.037 ± 0.001
Heteroskedastic	EBM	0.284 ± 0.004	0.176 ± 0.002	0.105 ± 0.001
	GAMI-Net	0.304 ± 0.010	0.133 ± 0.005	0.078 ± 0.005
	ELAAN-I	0.215 ± 0.008	0.087 ± 0.002	0.042 ± 0.001

of basis elements is too small (underfitting) or too large (overfitting). When the number of bases elements is large, it is important to use smoothing for regularization.

S4.2.2. Skewed or heteroskedastic error distributions (Synthetic data). We study how our model performs when the error distribution is (i) skewed, (ii) heteroskedastic. For (i), we consider a log-normal distribution for the error: $\epsilon \sim \mathcal{LN}(-1, 0.2546)$. For (ii), we consider a normal distribution for the error: $\epsilon \sim \mathcal{N}(0, 0.5092g_2(x_5))$, where the standard deviation is a function of the 5-th covariate in \mathbf{x} . We compare average ISE for ELAAN-I with EBM and GAMI-Net in these scenarios in Table S2. We can observe that ELAAN-I consistently outperforms both EBM and GAMI-Net even when the error distributions are not normally distributed. As expected, we observe a small drop in performance in both skewed and heteroskedastic settings compared to the normal distribution setting. We do not observe any degradation in support recovery metric in Table S3 under skewed setting; however, we do observe a drop in support recovery F1-scores in the heteroskedastic setting. For example, the F1-scores for main and interaction effects for ELAAN-I are 96.4% and 81.7% in the heteroskedastic setting for $N_{\text{train}} = 400$ compared to 97.4% and 87.3% in the normal distribution setting.

TABLE S3
Support recovery metrics for ELAAN-I, EBM and GAMI-Net when the error distribution is normal, skewed or heteroskedastic.

ϵ -distribution	N_{train}	Model	F1(main)	F1(interactions)
Skewed	100	EBM	57.14 ± 0.00	50.81 ± 1.86
		GAMI-Net	61.72 ± 0.84	21.39 ± 1.32
		ELAAN-I	86.17 ± 1.11	38.80 ± 2.95
	200	EBM	57.14 ± 0.00	73.91 ± 2.12
		GAMI-Net	59.21 ± 0.36	31.84 ± 1.52
		ELAAN-I	92.12 ± 0.83	71.63 ± 1.91
	400	EBM	57.14 ± 0.00	83.18 ± 1.92
		GAMI-Net	57.63 ± 0.20	43.33 ± 2.57
		ELAAN-I	97.01 ± 0.60	86.66 ± 1.09
Heteroskedastic	100	EBM	57.14 ± 0.00	49.96 ± 1.88
		GAMI-Net	61.55 ± 1.40	19.71 ± 2.03
		ELAAN-I	85.53 ± 1.11	40.40 ± 2.86
	200	EBM	57.14 ± 0.00	67.01 ± 2.09
		GAMI-Net	59.61 ± 0.58	32.89 ± 1.69
		ELAAN-I	90.72 ± 0.96	71.71 ± 1.54
	400	EBM	57.14 ± 0.00	81.22 ± 1.92
		GAMI-Net	58.42 ± 0.54	35.82 ± 2.93
		ELAAN-I	96.41 ± 0.65	81.75 ± 1.20

S4.3. *Tuning Details.*

S4.3.1. *Tuning Details for the Simulation in Section 4.1.* We use 100 replications for each simulation setting, i.e., settings with different training set sizes, error distributions etc. For each replication, we select the best hyperparameters via 5-fold cross-validation on the training set. We use mean squared error as the tuning criterion. Next, we run the model on the full training set with the best hyperparameters to compute ISE performance on the test set.

For EBM and GAMI-Net, we tune the number of interactions in the range $[1, 45]$ for 50 trials. For GAMI-Net, we used 32 batch-size, 0.0001 learning rate, 500 epochs (for each stage) and 0.0 loss threshold.

For ELAAN-I and ELAAN-H, we used 10 knots for the main effects and 5 knots in each coordinate for the interaction effects (leading to $5 \times 5 = 25$ knots). For ELAAN-I, we tuned $\lambda_1 \in \{10^{-6}, \dots, 10^{-2}\}$ and $\lambda_2 \in \{10^{-5}, \dots, 10^{-1}\}$ with warm-starts. For ELAAN-H, we tuned $\lambda_1 \in \{10^{-6}, \dots, 10^{-2}\}$ and $\lambda_2 \in \{10^{-4}, \dots, 1\}$, $\tau \in \{0.01, \dots, 1\}$ with warm-starts.

S4.3.2. *Tuning Details for the Simulation in Section 4.2.* We use 25 replications for each simulation setting. For each replication, we select the best hyperparameters via validation tuning, using a validation set of size 2,000 with the mean squared error as the tuning criterion. Next, we run the model on the full training set with the best hyperparameters to compute ISE performance on the test set.

For EBM, we tune the number of interactions in the range $[1, 100]$. For GAMI-Net, we tuned the model with number of interactions in the set $\{5, 50\}$. For GAMI-Net, we used 200 batch-size, 0.0001 learning rate, 500 epochs (for each stage) and 0.0 loss threshold.

For ELAAN-I and ELAAN-H, we used 10 knots for the main effects and 6 knots in each coordinate for the interaction effects (leading to $6 \times 6 = 36$ knots). For ELAAN-I, we tuned $\lambda_1 \in \{10^{-7}, \dots, 10^{-3}\}$ and $\lambda_2 \in \{10^{-4}, \dots, 10^0\}$ with warm-starts. The ℓ_0 regularization path was terminated when the number of interactions reached 50. For ELAAN-H, we fix the smoothing parameter λ_1 to the optimal value available from ELAAN-I and tuned $\lambda_2 \in \{10^{-2}, \dots, 10^2\}$ and $\tau \in \{0.01, \dots, 1\}$ with warm-starts. For ELAAN-I and ELAAN-H, we also considered three choices for α in the set $\{1.0, 1.5, 2.0\}$.

For ELAAN-H, our algorithm, outlined in S3, approximately solves the problem under hierarchy with ℓ_0 by solving the convex relaxation for computational reasons. From variable selection perspective, especially in the correlated setting considered in this simulation, the solution to the convex relaxation can overestimate the number of effects in the model e.g., the number of interactions. Hence, it can be beneficial to consider a solution along the regularization path with smaller number of selected components, but lies within a standard error of the best solution. The numbers reported for prediction error and support recovery for ELAAN-H in the Table 4 correspond to this choice of solution. This practice is common when using convex relaxations such as lasso in linear models.

S5. **Data Analysis: Additional Details.**

S5.1. *Definition of important Census/American Community Survey variables.*

S5.1.1. *Definition of the variables in Figure 3.*

- Tot_Population_ACS_13_17: U.S. resident population includes everyone who meets the ACS residence rules in the tract at the time of the ACS interview.
- pct_Prs_Blw_Pov_Lev_ACS_13_17: Percentage of the ACS eligible population that are classified as below the poverty level given their total family or household income within the last year.

- pct_College_ACS_13_17: The percentage of the ACS population aged 25 years and over that have a college degree or higher.
- pct_Not_HS_Grad_ACS_13_17: The percentage of the ACS population aged 25 years and over that are not high school graduates and have not received a diploma or the equivalent.
- pct_Pop_5_17_ACS_13_17: The percentage of the ACS population that is between 5 and 17 years old.
- pct_Pop_18_24_ACS_13_17: The percentage of the ACS population that is between 18 and 24 years old.
- pct_Pop_25_44_ACS_13_17: The percentage of the ACS population that is between 25 and 44 years old.
- pct_Pop_45_64_ACS_13_17: The percentage of the ACS population that is between 45 and 64 years old.
- pct_Pop_65plus_ACS_13_17: The percentage of the ACS population that is 65 years old or over.
- pct_Hispanic_ACS_13_17: The percentage of the ACS population that identify as "Mexican", "Puerto Rican", "Cuban", or "another Hispanic, Latino, or Spanish origin".
- pct_NH_White_alone_ACS_13_17: The percentage of the ACS population that indicate no Hispanic origin and their only race as "White" or report entries such as Irish, German, Italian, Lebanese, Arab, Moroccan, or Caucasian.
- pct_NH_Black_alone_ACS_13_17: The percentage of the ACS population that indicate no Hispanic origin and their only race "Black, African American, or Negro" or report entries such as African American, Kenyan, Nigerian, or Haitian.
- pct_ENG_VW_ACS_13_17: The percentage of all ACS occupied housing units where no one ages 14 years and over speaks English only or speaks English "very well".
- pct_Othr_Lang_ACS_13_17: The percentage of the ACS population aged 5 years and over that speaks a language other than English at home.
- pct_Diff_HU_1yr_Ago_ACS_13_17: The percentage of the ACS population aged 1 year and over that moved from another residence in the U.S. or Puerto Rico within the last year.
- avg_Tot_Prns_in_HHD_ACS_13_17: The average number of persons per ACS occupied housing unit. This was calculated by dividing the total household population in the ACS by the total number of occupied housing units in the ACS.
- pct_Sngl_Prns_HHD_ACS_13_17: The percentage of all ACS occupied housing units where a householder lives alone.
- pct_Female_No_HB_ACS_13_17: The percentage of all ACS occupied housing units with a female householder and no spouse of householder present.
- pct_Rel_Under_6_ACS_13_17: The percentage of 2010 ACS family-occupied housing units with a related child under 6 years old; same-sex couple households with no relatives of the householder present are not included in the denominator.
- pct_Vacant_Units_ACS_13_17: The percentage of all ACS housing units where no one is living regularly at the time of interview; units occupied at the time of interview entirely by persons who are staying two months or less and who have a more permanent residence elsewhere are classified as vacant.
- pct_Renter_Occp_HU_ACS_13_17: The percentage of ACS occupied housing units that are not owner occupied, whether they are rented or occupied without payment of rent.
- pct_Owner_Occp_HU_ACS_13_17: The percentage of ACS occupied housing units with an owner or co-owner living in it.
- pct_Single_Unit_ACS_13_17: The percentage of all ACS housing units that are in a structure that contains only that single unit.

- `Med_HHD_Inc_ACS_13_17`: Median ACS household income for the tract.
- `Med_House_Value_ACS_13_17`: Median of ACS respondents' house value estimates for the tract.
- `pct_HHD_Moved_in_ACS_13_17`: The percentage of all ACS occupied housing units where the householder moved into the current unit in the year 2010 or later.
- `pct_NO_PH_SRVC_ACS_13_17`: The percentage of ACS occupied housing units that do not have a working telephone and available service.
- `pct_HHD_No_Internet_ACS_13_17`: Percentage of ACS households that have no Internet access.
- `pct_HHD_w_Broadband_ACS_13_17`: Percentage of ACS households that have broadband Internet access.
- `pct_Pop_w_BroadComp_ACS_13_17`: Percentage of people that live in households that have both broadband Internet access and a computing device of any kind in the ACS.
- `pct_URBANIZED_AREA_POP_CEN_2010`: The percentage of the 2010 Census total population that lives in a densely settled area containing 50,000 or more people.
- `pct_MrdCple_HHD_ACS_13_17`: The percentage of all ACS occupied housing units where the householder and his or her spouse are listed as members of the same household; does include same sex married couples.
- `pct_NonFamily_HHD_ACS_13_17`: The percentage of all ACS occupied housing units where a householder lives alone or with non relatives only; includes unmarried same-sex couples where no relatives of the householder are present.
- `pct_MLT_U2_9_STRC_ACS_13_17`: The percentage of all ACS housing units that are in a structure that contains two to nine housing units.
- `pct_MLT_U10p_ACS_13_17`: The percentage of all ACS housing units that are in a structure that contains 10 or more housing units.
- `Civ_labor_16plus_ACS_13_17`: Number of civilians ages 16 years and over at the time of the interview that are in the labor force in the ACS.
- `pct_Civ_emp_16plus_ACS_13_17`: The percentage of ACS civilians ages 16 years and over in the labor force that are employed.
- `pct_One_Health_Ins_ACS_13_17`: The percentage of the ACS population that have one type of health insurance coverage, including public or private.
- `pct_TwoPHealthIns_ACS_13_17`: The percentage of the ACS population that have two or more types of health insurance.
- `pct_No_Health_Ins_ACS_13_17`: The percentage of the ACS population that have no health insurance, public or private.

S5.1.2. Definition of the variables in Figure 7(b).

- `pct_Prs_Blw_Pov_Lev_ACS_13_17`: The percentage of the ACS eligible population that are classified as below the poverty level given their total family or household income within the last year, family size, and family composition.
- `Age5p_German_ACS_13_17`: Number of people ages 5 years and over who speak English less than "very well" and speak German at home in the ACS. Examples include Luxembourgian.
- `pct_NH_White_alone_ACS_13_17`: The percentage of the ACS population that indicate no Hispanic origin and their only race as "White" or report entries such as Irish, German, Italian, Lebanese, Arab, Moroccan, or Caucasian.
- `pct_Owner_Occp_HU_ACS_13_17`: The percentage of ACS occupied housing units with an owner or co-owner living in it.
- `pct_Diff_HU_1yr_Ago_ACS_13_17`: The percentage of the ACS population aged 1 year and over that moved from another residence in the U.S. or Puerto Rico within the last year.

- `pct_Vacant_Units_CEN_2010`: The percentage of all 2010 Census housing units that have no regular occupants on Census Day; housing units with its usual occupants temporarily away (such as on vacation, a business trip, or in the hospital) are not considered vacant, but housing units temporarily occupied on Census Day by people who have a usual residence elsewhere are considered vacant.
- `pct_College_ACS_13_17`: The percentage of the ACS population aged 25 years and over that have a college degree or higher.
- `pct_Single_Unit_ACS_13_17`: The percentage of all ACS housing units that are in a structure that contains only that single unit.
- `pct_Sngl_Prns_HHD_Cen_2010`: The percentage of all 2010 Census occupied housing units where a householder lives alone.
- `pct_NH_Black_alone_CEN_2010`: The percentage of the 2010 Census total population that indicate no Hispanic origin and their only race as "Black, African American, or Negro" or report entries such as African American, Kenyan, Nigerian, or Haitian.
- `pct_Tot_Occp_Units_ACS_13_17`: The percentage of all ACS housing units that are classified as the usual place of residence of the individual or group living in it.
- `pct_Not_HS_Grad_ACS_13_17`: The percentage of the ACS population aged 25 years and over that are not high school graduates and have not received a diploma or the equivalent.
- `pct_NoHealthIns1964_ACS_13_17`: Percentage of people age 19 to 64 with no health insurance in the ACS.
- `pct_US_Cit_Nat_ACS_13_17`: The percentage of the ACS population who are citizens of the United States through naturalization.
- `pct_NH_Asian_alone_Cen_2010`: The percentage of the 2010 Census total population that indicate no Hispanic origin and their only race as "Asian Indian", "Chinese", "Filipino", "Korean", "Japanese", "Vietnamese", or "Other Asian".
- `pct_Pop_25yrs_Over_ACS_13_17`: The percentage of the ACS population who are ages 25 years and over at time of interview.
- `pct_Not_MrdCple_HHD_Cen_2010`: The percentage of all 2010 Census occupied housing units where no spousal relationship is present.
- `Not_HS_Grad_ACS_13_17`: The percentage of the ACS population aged 25 years and over that are not high school graduates and have not received a diploma or the equivalent.
- `NH_White_alone_CEN_2010`: Number of people who indicate no Hispanic origin and their only race as "White" or report entries such as Irish, German, Italian, Lebanese, Arab, Moroccan, or Caucasian in the 2010 Census population.